Available online at www.sciencedirect.com
SCIENCE DIRECT®
Advances in Water Resources 27 (2004) 361–382
Advances in Water Resources
www.elsevier.com/locate/advwatres

A fully coupled physically-based spatially-distributed model for evaluating surface/subsurface flow

Sorab Panday, Peter S. Huyakorn *

HydroGeoLogic Inc., 1155 Herndon Pkwy, Ste 900, Herndon, VA 20170, USA

Received 19 December 2003; accepted 4 February 2004

Abstract

A physically-based, spatially-distributed model is presented for simulation of surface/subsurface flow and the interactions between these domains. The model is designed for practical application to a wide variety of hydrologic evaluations, at various scales of simulation. The system is represented by the three-dimensional saturated–unsaturated flow equation for the subsurface, coupled with the diffusion wave equation for areal overland flow, both of which are coupled with the diffusion wave equation for flow through a network of streams and channels, including hydraulic structures. Ground surface unevenness at the grid scale is incorporated via the concept of detention storage, and thick vegetation or urban features are included via an obstruction storage exclusion term. Evapotranspiration from the surface and subsurface are modeled using land cover and climatic factors to define the complete water budget using a physically-based formulation. The system of equations is discretized using a fully implicit procedure, with the Newton–Raphson method to handle non-linearities efficiently. Robustness, stability and accuracy of solution are obtained for a wide variety of cases including dry systems and large surface/subsurface interaction fluxes. Adaptive time-stepping schemes and under-relaxation formulas further alleviate the computational burden. Verification and application examples demonstrate the need for a rigorous, fully-coupled solution to the set of equations, for complete hydrologic-cycle analysis.

1. Introduction

Problems involving strong interactions between surface-water and groundwater regimes, as well as investigations of conjunctive water management issues, necessitate coupled simulation of the surface and subsurface flow regimes. Characterization of flow processes individually within these regimes is well established. For example, robust and efficient techniques for modeling saturated–unsaturated flow in the subsurface are discussed by Huyakorn and Pinder [20], Huyakorn et al. [21], Panday et al. [27] and Forsyth et al. [13]; spatially distributed modeling of overland runoff is investigated by Zhang and Cundy [47], Fennema and Chaudhry [11], Gottardi and Venutelli [16] and Singh and Bhallamudi [33]; and modeling of flow through channel or river networks is presented by Schaffranek et al. [31], Chaudhry [6] and USACE [38]. Attempts have also been made to link (via time-lagging or iterative coupling) some or all of these flow regimes to analyze more complete flow behavior. For instance, Woolisher et al. [46] and Smith et al. [35] describe a model that links overland flow, channel flow, interception losses, and analytical solutions for infiltration losses, whereas Senarath et al. [32] describe a model for two-dimensional overland flow that accounts for evapotranspiration losses and uses analytical solutions for infiltration losses. Prudic [29], Swain and Wexler [36], and Walton et al. [43] discuss linking of the channel flow domain with the saturated subsurface regime (i.e., with groundwater flow); Pinder and Sauer [28], Akan and Yen [1], Singh and Bhallamudi [34], and Morita and Yen [26] investigate linking of the overland regime with the saturated–unsaturated subsurface regime; and Freeze [14,15], Govindaraju and Kavvas [17] and Graham and Refsgaard [18] examine linking of subsurface, overland, and channel flow regimes for determining the general response of a watershed due to interactions among all regimes. Linked solutions to these domains are however, numerically weak and unreliable [9,23] and a fully implicit coupling of the overland and subsurface flow domains was explored by VanderKwaak [39] and

* Corresponding author.
E-mail addresses: smp@hgl.com (S. Panday), psh@hgl.com (P.S. Huyakorn).

0309-1708/$ - see front matter © 2004 Elsevier Ltd. All rights reserved.
doi:10.1016/j.advwatres.2004.02.016

VanderKwaak and Loague [40]. The fully coupled solution outperforms linked/iteratively coupled methods in terms of computational efficiency for highly interactive systems. It is also an invaluable tool that enables rigorous examination/testing of the accuracy and sufficiency of linked modeling methods widely applied today.

The current study presents a fully coupled approach to the solution of subsurface flow, overland flow, and flow through a network of channels (or small-scale surface-water features that may be treated with a lower dimensionality). The model presented provides innovative extensions to the standard flow equations to account for urban or agricultural features at various scales. Equations governing overland and channel flow are modified to include effects of depression storage and obstruction storage exclusion, to account for flow within urban or agricultural settings at small and large scales. The surface/subsurface interactions also include depression storage effects as physical processes that affect flow across the land surface. Channel geometries may be regular (rectangular, trapezoidal, or circular to account for pipes) or irregular, and leakances may vary with flow-depth within the channel to allow for simulation of various natural or man-made conditions. Engineered hydraulic structures are also incorporated within the channel flow regime by use of tabulated flow vs head relations of a general nature that can accommodate a wide variety of weirs, culverts, manholes, drop-structures, bridges, gates, pumps, etc. Flow across structures may further be regulated by a set of operational or shift-work rules. Small surface-water bodies within a channel/river system are accurately depicted using their storage-area relations to accommodate fine details in otherwise large-scale simulations. Reference evapotranspiration estimates may be input from pan data or calculated from climatic and crop information for a fully mechanistic approach to hydrologic-cycle analysis. Detailed models for plant transpiration based on crop/land-cover and soil moisture information are presented along with various evaporation models that are applicable to a variety of situations, for realistic estimates of long-term water budget evaluations. Complexity of simulation may be incorporated on an as-needed basis, even within a single model. Therefore, each part of the domain for a given simulation can be specified with its own degree of complexity, to allow for a wide range of applicability including flood forecasting, water resource assessment, watershed hydrologic analysis, and flood plain/fluvial hydraulic analysis.

The system of equations is discretized in space using finite-difference and finite-volume considerations, and in time using a fully implicit procedure. Newton–Raphson linearization is used to handle the non-linearities. The model can simulate fully dry regions, as well as regions with large surface, subsurface, or interaction fluxes in an efficient and robust manner. The fully coupled solution technique is supplemented with linked/iteratively coupled approaches to provide a framework for comparison between these solution techniques. Numerical handling of terms of the conductance matrix and of evapotranspiration are discussed, and verification examples are presented that highlight the applicability and accuracy of the mathematical model and solution techniques.

2. Governing processes and equations

The equations governing flow of water for hydrologic-cycle modeling are presented below. Processes describing water movement in the subsurface and surface flow domains are first discussed, followed by interaction processes and processes related to evapotranspiration, that span all domains.

2.1. Subsurface flow

A rigorous approach satisfying flow continuity in three-dimensions in both the saturated and unsaturated zones of the subsurface is required for robust and reliable solutions for subsurface flow under a variety of general flow conditions. This is provided by the mixed form of the Richard's equation for variably-saturated subsurface flow expressed as [27]

$$\begin{aligned}&\frac{\partial}{\partial x}\left(K_{xx}k_{\mathrm{rw}}\frac{\partial h_{\mathrm{G}}}{\partial x}\right)+\frac{\partial}{\partial y}\left(K_{yy}k_{\mathrm{rw}}\frac{\partial h_{\mathrm{G}}}{\partial y}\right)\\&\quad+\frac{\partial}{\partial z}\left(K_{zz}k_{\mathrm{rw}}\frac{\partial h_{\mathrm{G}}}{\partial z}\right)-W+q_{\mathrm{go}}+q_{\mathrm{gc}}\\&\quad=\phi\frac{\partial S_{\mathrm{w}}}{\partial t}+S_{\mathrm{w}}S_{\mathrm{s}}\frac{\partial h_{\mathrm{G}}}{\partial t}\end{aligned}\tag{1}$$

subject to evapotranspiration and various other boundary conditions, where x, y, and z are Cartesian coordinates (L); K_{xx}, K_{yy}, and K_{zz} are the principal components of hydraulic conductivity along the x, y, and z axes, respectively (LT^{-1}); k_{rw} is the relative permeability which is a function of water saturation as provided by the relative permeability curve; h_{G} is the hydraulic head of the subsurface flow system (L); W is a volumetric flux per unit volume of the subsurface domain and represents sources and/or sinks of water (T^{-1}); q_{go} is the flux per unit volume of subsurface from the 2-D overland flow domain (T^{-1}); q_{gc} is the flux per unit volume of subsurface from the 1-D channel or surface-water feature domain (T^{-1}); ϕ is the porosity; S_{w} is the degree of water saturation and is determined by the moisture retention curve as a function of the pressure head, ψ ($\psi = h_{\mathrm{G}} - z$, where $z =$ nodal elevation in a vertically upward coordinate system); S_{s} is the specific storage of the porous material (L^{-1}); and t is time (T). Dimensions of this equation are volumetric flux per unit

volume (T^{-1}). Functional forms of the relative permeability curve are provided by Brooks and Corey [4] as

$$k_{\mathrm{rw}} = S_{\mathrm{e}}^{b} \tag{2}$$

and by van Genuchten [42] as

$$k_{\mathrm{rw}} = S_{\mathrm{e}}^{1/2}[1-(1-S_{\mathrm{e}}^{1/\gamma})^{\gamma}]^2 \tag{3}$$

where b and γ are empirical parameters; and S_{e} is the effective water saturation defined as $S_{\mathrm{e}} = (S_{\mathrm{w}} - S_{\mathrm{wr}})/(1 - S_{\mathrm{wr}})$, where S_{wr} is the residual water saturation. The Brooks–Corey expression produces similar curves to the van Genuchten function when the following relation between their parameters is applied:

$$b = 1 + 2/\gamma \tag{4}$$

This conversion is useful to determine the Brooks–Corey exponent term when the van Genuchten parameters are known. Use of the Brooks–Corey function might benefit the non-linear iterations since it is often less non-linear than its corresponding van Genuchten function. A functional form of the moisture retention curve is given by van Genuchten et al. [41] as

$$S_{\mathrm{e}} = \frac{S_{\mathrm{w}} - S_{\mathrm{wr}}}{1 - S_{\mathrm{wr}}} = \begin{cases} \frac{1}{[1+(\alpha\psi)^{\beta}]^{\gamma}} & \text{for } \psi < 0 \\ 1 & \text{for } \psi \geqslant 0 \end{cases} \tag{5}$$

where α and β are fitting parameters. The parameters β and γ are related by $\gamma = 1 - 1/\beta$. The Brooks–Corey and van Genuchten functions for the moisture retention and relative permeability characteristics may be obtained by curve-fitting to laboratory measurements, by correlation to soil type, or by consulting in soils databases.

2.2. Overland flow

Overland flow/runoff is characterized by the two-dimensional diffusion wave approximation to the St. Venant equations governing shallow-water flow, derived by Gottardi and Venutelli [16] as

$$\frac{\partial h_{\mathrm{O}}}{\partial t} - \frac{\partial}{\partial x}\left(dk_x \frac{\partial h_{\mathrm{O}}}{\partial x}\right) - \frac{\partial}{\partial y}\left(dk_y \frac{\partial h_{\mathrm{O}}}{\partial y}\right) - dq_{\mathrm{og}} - dq_{\mathrm{oc}} = 0 \tag{6}$$

subject to precipitation, evaporation and various other boundary conditions, where $h_{\mathrm{O}}(= z_{\mathrm{O}} + d)$ is the water surface elevation (L); d is the depth of flow (L); z_{O} is the bed (land surface) elevation (L); q_{og} is the flux per unit volume of overland flow domain from the subsurface (T^{-1}), where $q_{\mathrm{go}} = -q_{\mathrm{og}}$; and q_{oc} is the flux per unit volume of overland flow domain from the channel (T^{-1}). The dimensions of this equation are volumetric flux per unit area (vertically integrated over the depth of the overland flow domain) (LT^{-1}). The conductance terms k_x and k_y (LT^{-1}), result from manipulation of the St. Venant equations and are given for the Manning equation by Gottardi and Venutelli [16] as

$$k_i = \frac{d^{2/3}}{n_i}\frac{1}{[\partial h_{\mathrm{O}}/\partial s]^{1/2}} \quad (i = x, y) \tag{7}$$

where the index i represents the x and y coordinate directions. The friction slopes may alternatively be expressed by the Chezy or Darcy–Weisbach equations, and the corresponding conductance terms may be similarly computed as

$$k_i = C_i d^{1/2}\frac{1}{[\partial h_{\mathrm{O}}/\partial s]^{1/2}} = \sqrt{\frac{8g}{f_i}}\, d^{1/2}\frac{1}{[\partial h_{\mathrm{O}}/\partial s]^{1/2}} \quad (i = x, y) \tag{8}$$

where g is gravity (LT^{-2}); Manning's coefficient, n_i, has units of $T/L^{1/3}$; Chezy's coefficient, C_i, has units of $L^{1/2}/T$; Darcy–Weisbach friction factor, f_i, is dimensionless; and s is the length along the direction of maximum local slope. The relationship between these coefficients is as follows:

$$C_i = \frac{d^{1/6}}{n_i} = \sqrt{\frac{8g}{f_i}} \tag{9}$$

The Darcy–Weisbach friction factor may be input from average flow conditions, or they may be computed internally from a Moody diagram which is approximated for laminar flow by Akan and Yen [1] as

$$f_i = C_{\mathrm{L}}/Re_i \tag{10}$$

where C_{L} is a constant that depends on rainfall intensity and is expressed as

$$C_{\mathrm{L}} = 24 + 27.162r^{0.407} \tag{11}$$

where r is the rainfall intensity in in./h; and Re_i is the Reynolds number in direction i given as

$$Re_i = \frac{V_i d}{v} \tag{12}$$

where v is the kinematic viscosity; and V_i is the depth-averaged linear velocity in direction i.

2.3. Channel flow and surface-water features

All features of the land surface can conceptually be represented by the overland flow surface, including surface-water features such as ponds, lakes, reservoirs, rivers, streams and canals, by use of a sufficiently small discretization. However, there is a practical issue of scale in regional simulations, whereby a minimum limit must be set on the areal grid-block size of the overland flow surface as well as of the subsurface layers. Therefore, to accurately simulate surface-water features which are smaller than the associated grid-block dimensions, and to convey water through canals or conveyance structures (whose widths are much finer than the grid-block

scale or whose orientation may not conform well with the finite difference structure), a surface-water features/channel flow layer is added to the surficial model layer. This layer is characterized by a network of one-dimensional channels/features which communicate water within the network, as well as between it and the overland flow and subsurface domains.

Flow through a network of rivers and channels is characterized by the one-dimensional diffusion wave approximation to the St. Venant equations, which is derived in a similar manner to its two-dimensional counterpart and is expressed as

$$B\frac{\partial h_C}{\partial t} - \frac{\partial}{\partial \ell}\left(\kappa_l \frac{\partial h_C}{\partial \ell}\right) - Aq_{cg} - Aq_{co} = 0 \tag{13}$$

subject to precipitation, evaporation and various other boundary conditions, where B is the top width (L); $h_C(= z_C + d)$ is the water surface elevation in the channel (L); d is the flow depth in the channel (L); z_C is the channel bed elevation (L); l is the length along the direction of flow (L); κ_ℓ is the conductance term along the length of the channel (L^3T^{-1}) resulting from manipulation of the one-dimensional St. Venant equations; q_{cg} is the flux per unit volume of channel flow domain from the subsurface (T^{-1}), where $q_{cg} = -q_{gc}$; and q_{co} is the flux per unit volume of channel flow domain from the overland flow domain (T^{-1}), where $q_{co} = -q_{oc}$. Dimensions of this equation are volumetric flux per unit length of channel (L^2/T), integrated over the channel's cross-sectional area of flow, $A(L^2)$. At junctions, the flow term (second term in Eq. (13)) is expressed in a finite-volume manner between all channel segments that intersect at the junction. The friction slope may be approximated by Manning's formula, by Chezy's equation, or by the Darcy–Weisbach relation to provide the respective conductance terms as

$$\kappa_l = \frac{1}{n_l}\cdot\frac{A^{5/3}}{P^{2/3}}\cdot\frac{1}{[\partial h_C/\partial \ell]^{1/2}} = C_\ell \cdot \frac{A^{3/2}}{P^{1/2}}\cdot\frac{1}{[\partial h_C/\partial \ell]^{1/2}} = \sqrt{8g/f_\ell}\cdot\frac{A^{3/2}}{P^{1/2}}\cdot\frac{1}{[\partial h_C/\partial \ell]^{1/2}} \tag{14}$$

where P is the wetted perimeter of the channel segment (L). The relationship between these coefficients is as follows:

$$C_\ell = \frac{A^{1/6}}{n_\ell P^{1/6}} = \sqrt{\frac{8g}{f_\ell}} \tag{15}$$

and the friction factors may be average inputs or calculated via Eq. (10), as applied along the direction of flow of the channel. Various regular geometries may be accommodated in the formulation by providing the appropriate formulas to calculate A and P. Hence, from geometric considerations it follows that for a wide rectangle,

$$A = Bd \tag{16a}$$

For a trapezoidal channel,

$$A = \left[B + d\frac{(SR + SL)}{2}\right]d \tag{16b}$$

For a circular conduit when $d < R$,

$$A = R^2\cos^{-1}\left(\frac{R-d}{R}\right) - (R-d)\sqrt{R^2 - (R-d)^2} \tag{16c}$$

For a circular channel with $R < d < 2R$,

$$A = R^2\left[\pi - \cos^{-1}\left(\frac{d-R}{R}\right)\right] + (d-R)\sqrt{R^2 - (R-d)^2} \tag{16d}$$

and for a circular channel with $d > 2R$,

$$A = \pi R^2 \tag{16e}$$

The perimeter is obtained as follows. For a wide rectangle,

$$P = B \tag{17a}$$

For a trapezoidal channel,

$$P = B + d[(1 + SR^2)^{1/2} + (1 + SL^2)^{1/2}] \tag{17b}$$

For a circular conduit when $d < R$,

$$P = 2R\cos^{-1}\left(\frac{R-d}{R}\right) \tag{17c}$$

For a circular channel with $R < d < 2R$,

$$P = 2R\left[\pi - \cos^{-1}\left(\frac{d-R}{R}\right)\right] \tag{17d}$$

and for a circular channel with $d > 2R$,

$$P = 2\pi R + 2(d - 2R) \tag{17e}$$

where the geometric parameters are defined in Fig. 1. Note that the Eq. (17e) includes a Preisman slot concept to accommodate pressurized flow within circular pipes. An irregular channel cross-section or a composite channel section is implemented by directly providing appropriate tabular values of A, P, and B, as noted in Fig. 1, which may be generated by a pre-processor from observed or design conditions.

2.4. Treatment of depression storage and storage exclusion

To accommodate urban or agricultural settings at large scales of analysis, the above equations for the 2-D overland flow (runoff) domain and the 1-D channel (surface-water feature) flow domain are modified to include terms for depression storage and for obstruction

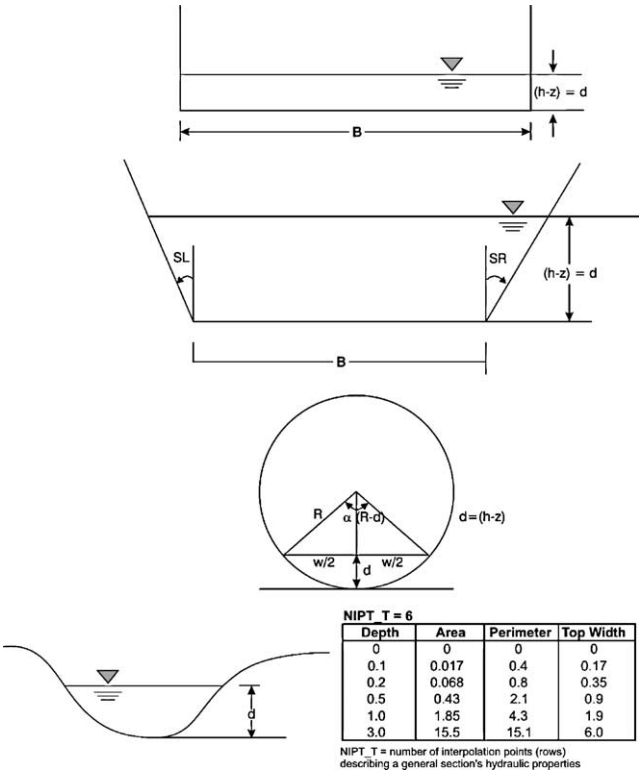

NIPT_T = 6

Depth	Area	Perimeter	Top Width
0	0	0	0
0.1	0.017	0.4	0.17
0.2	0.068	0.8	0.35
0.5	0.43	2.1	0.9
1.0	1.85	4.3	1.9
3.0	15.5	15.1	6.0

NIPT_T = number of interpolation points (rows) describing a general section's hydraulic properties

Fig. 1. Channel representation of wide rectangle, trapezoidal, circular conduit, and general cross-sections.

storage exclusion. As described in Eqs. (6) and (13), it is assumed that flow occurs over a flat plane as shown in Fig. 2a. For unlined river beds or natural streams, the setting is much different as shown in Fig. 2b, with flow occurring between the obstructions in an averaged sense over the cross-sectional area. The case of Fig. 2b is also applicable to the two-dimensional overland flow surface in urban environments with man-made obstructions such as buildings. Only if the flow of water is high enough to completely cover the obstructions is the full area available for flow and storage of water. If not accounted for, lower flow-depths and incorrect discharge would be predicted for systems having significant obstruction impact. The storage capacity that is reduced by the presence of these features is termed obstruction storage exclusion. In addition to the storage term, these features may also affect the horizontal flow conductance term due to larger frictional resistance and small scale energy dissipation over the obstruction surface.

Fig. 2c shows the concept of depression storage (which includes rills, furrows and other detention features) which is an important factor accounting for ground unevenness as compared to the scale of the model grid-block. This is the amount of storage that must be filled before lateral flow can occur in any direction from that grid-block. Microtopographic relief is included in depression storage and can have a substantial impact on hydrograph shape [45]. Finally, for agricultural plots or grassy channels (as shown in Fig. 2d), the effects of depressions as well as of storage exclusion must be taken into account in the model's

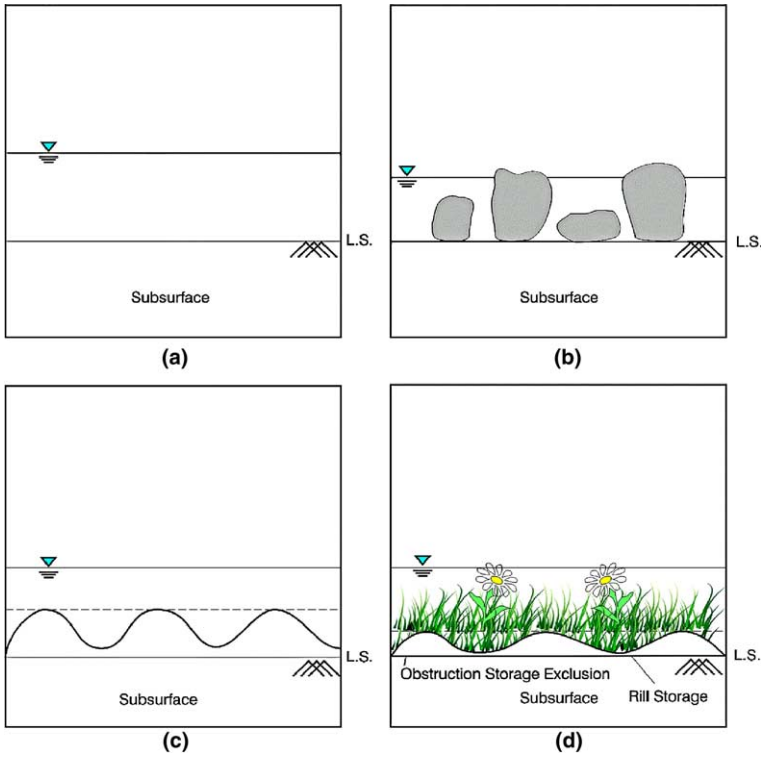

Fig. 2. Treatment of storage terms for various settings.

storage term as well as in the horizontal flow conductance term.

The storage effects of depression storage and obstruction storage exclusion are modeled by assuming that the geometry of depressions and exclusions combined has a maximum elevation and that the horizontal area covered by surface-water varies between zero and full area as the water level rises from land surface (LS, defined here as the bottom of the depressions) up to this maximum elevation $(\mathrm{LS} + h_{\mathrm{ds}} + h_{\mathrm{os}})$ as shown in Fig. 3. The variation of area covered by surface-water with depth between (LS) and $(\mathrm{LS} + h_{\mathrm{ds}} + h_{\mathrm{os}})$ is expressed as a 'volumetric height' defined as the height from LS of an equivalent volume of water without depressions or obstructions. The 'volumetric height' is then used in the storage term of Eqs. (6) and (13) instead of the surface-water depth, to account for the reduced available storage volumes. A parabolic curve is used to express the volumetric height in terms of flow depth, the slope of which may be viewed as a porosity or void ratio which varies linearly between zero at an elevation of (LS) up to unity at the elevation $(\mathrm{LS} + h_{\mathrm{ds}} + h_{\mathrm{os}})$. Other functional forms may also be used; however, a parabolic variation provides for continuous derivatives at land surface and at the maximum storage height (h_{s}), thus assisting during numerical solution by Newton–Raphson or modified-Picard linearization methods. The heights of depression storage (h_{ds}) and of storage within the obstructions, (h_{os}) are physical parameters that geometrically represent the mean spacing (equivalent void space) within the respective storage elements as a function of flow depth. Initial estimates may be developed using statistical analysis of surface unevenness.

The horizontal flow conductance term is also affected by the presence of depressions and storage obstruction features. The depression storage height above land surface $(\mathrm{LS} + h_{\mathrm{ds}})$ is used as the reference elevation for flow depth calculation in the advection terms of Eqs. (6)–(17) when depression storage is modeled for a system. Thus, overland flow occurs only when the overland flow node's head is above an elevation of $(\mathrm{LS} + h_{\mathrm{ds}})$ i.e., when the overland domain's water level is above the depression storage elevation. The depression storage elevation may be different for the two principal areal directions to account for furrows or other plowed features. In addition, the conductance terms (k_x and k_y) can be multiplied by a factor K_{s} from the depression storage elevation to the height of obstruction storage exclusion to account for additional resistance losses for low flow conditions within the obstructions. The factor K_{s} varies from zero to unity as the depth of flow varies from $(\mathrm{LS} + h_{\mathrm{ds}})$ to $(\mathrm{LS} + h_{\mathrm{ds}} + h_{\mathrm{os}})$ within the obstruction zone. The same situation applies also to the channel flow domain. Note that when h_{ds} and h_{os} approach zero, the formulation approaches that of flow over a flat plane as depicted in Fig. 2a.

2.5. Treatment of interaction terms among domains

Flows between the subsurface, overland, and channel domains of the system are represented by the unit interactive fluxes presented in Eqs. (1), (6) and (13). The overland/subsurface interaction term q_{go} is the unit flux across the ground surface which, for grid cell of dimensions Δx and Δy, is computed as

$$q_{\mathrm{go}} V_{\mathrm{G}} = -k_{\mathrm{rgo}} (\Delta x \Delta y) K_{\mathrm{go}} (h_{\mathrm{G}} - h_{\mathrm{O}}) = Q_{\mathrm{go}} \tag{18}$$

where Q_{go} $(L^3 T^{-1})$ is the flux across the total area of the interface, from the overland flow domain to the subsurface (negative for flow out of the subsurface); the multiplier of subsurface elementary volume, V_{G}, accounts for q_{go} being a flux per unit volume of subsurface; and $K_{\mathrm{go}}(T^{-1})$ is the leakance across the ground surface to the modeled subsurface. This leakance may include a skin layer effect, or it may be defined as the vertical hydraulic conductivity of the topmost subsurface layer of nodes divided by its half-thickness (which represents the distance of flow for a block-centered

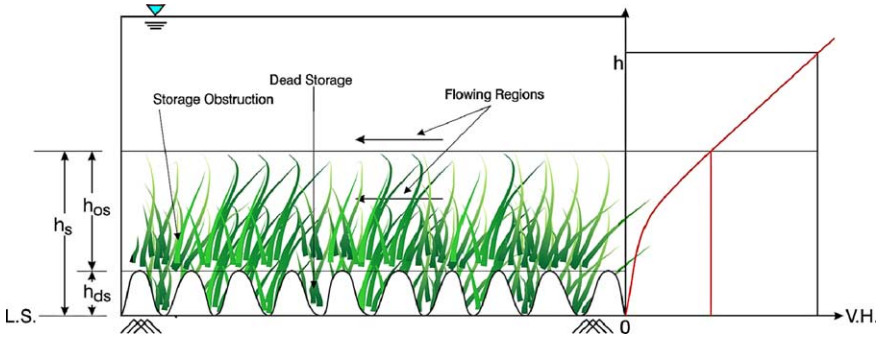

Fig. 3. Conceptual model for depression storage and obstruction storage exclusion. LS = land surface = elevation of top of underlying subsurface node; horizontal area available for storage of water at or below this height is zero for the overland node. h_{ds} = height of depression storage = height at which overland flow starts to occur. h_{os} = height of storage within obstructions. $h_{\mathrm{s}} = h_{\mathrm{ds}} + h_{\mathrm{os}}$ = maximum height over which area covered by surface-water goes from zero at LS, to unity at $\mathrm{LS} + h_{\mathrm{s}}$. VH = 'volumetric height' defined as the height from LS, of an equivalent volume of water without depressions or obstructions.

subsurface node). The term k_{rgo} varies between zero at land surface elevation (LS), and unity at the depression storage height above land surface (LS + h_{ds}); it accounts for the fraction of the total area that is wet when water level is within the depression height at any location.

The channel/subsurface interaction term q_{gc} is expressed as

$$q_{gc}V_G = -k_{rgc}(L_C P_{ups})K_{gc}(h_G - h_C) = Q_{gc} \tag{19}$$

where $Q_{gc}(L^3T^{-1})$ is the flux across the total area of the interface from the channel to the subsurface (negative for flow out of the subsurface); L_C is the channel segment length (L); and $K_{gc}(T^{-1})$ is the net leakance across the channel bed to the subsurface system, expressed as

$$K_{gc} = \frac{K_{eff}}{b} \tag{20}$$

where K_{eff} (LT^{-1}) is the effective conductivity of channel sediments; P_{ups} is the upstream wetted perimeter (L) obtained from Eq. (17) for the different segment geometries, where the larger of h_C or h_G is upstream and determines the associated wetted perimeter; and b is the effective thickness of the sediments (L) across which flow occurs to the subsurface node. The leakance of sediments (K_{eff}/b) may be input as a constant; however, the net flux across the domains depends on the upstream wetted perimeter. The term k_{rgc} varies between zero at channel bottom elevation and unity at the channel's depression storage height above the channel bottom, to account for the fraction of the total area that is wet when water level is within the depression storage height at any location.

For channels, the conductivity term K_{eff} may be a constant or may vary with flow-depth within the section. For instance, a concrete lined channel may have grassy overflow storage areas, the composite being treated as a channel section. For bed conductivity varying with flow-depth, the term K_{eff} is computed as

$$K_{eff} = \frac{\int_0^{Z_1} K(z)P(z)\,dz}{P_1(Z_1)} \tag{21}$$

where Z_1 is the computed depth of flow in the channel. Z_1 cannot be greater than the channel bank elevation, defined as the elevation above which the channel section interacts with the overland flow domain on which it is located (denoted later as Z_{BANK}). Discretely varying channel sediment leakances/conductivities commonly occur in engineered systems. For instance, the channel bed may have a conductivity value of K_1 from a depth of zero to depth z_1, with a conductivity value of K_2 for depths between z_1 and z_2, and a conductivity value of K_3 for depths between z_2 and z_3, and so on. The effective conductivity of the channel sediments for such a system is obtained by applying Eq. (21) on the discrete intervals to give:

$$K_{eff}(Z_1) = \frac{K_1P_1 + K_2(P_2 - P_1) + K_3(P(Z_1) - P_2)}{P(Z_1)} \tag{22}$$

where the depth of flow Z_1 lies between the depths z_2 and z_3 for the example shown in Eq. (22).

The interaction term between the channel and overland flow domains is expressed by the equations for flow over a wide rectangular weir. Fig. 4 shows two of the typical situations which may occur—one for a free-flowing weir, and one for a submerged weir—each represented by its own flow relationship. Note that the cases shown in this figure could be reversed, with the channel overflowing its banks. For free flowing conditions across the channel banks the flow is expressed as [30]

$$q_{oc}^{free}A_O h_O = C_d\frac{2}{3}\sqrt{2g}(2L_C)(h_u - Z_{BANK})^{3/2} = Q_{oc}^{free} \tag{23}$$

where Q_{oc} (L^3T^{-1}) is the flux across the total length of channel banks to/from the overland flow domain; C_d is a weir discharge coefficient (dimensionless); h_u is the upstream head between channel and overland systems (L), (h_u corresponds to h_O in Fig. 4); Z_{BANK} is the bank elevation (L) which may be at or above the overland flow surface elevation; the term 2 L_C denotes that interaction occurs over the length of both banks; and the multiplier of the overland domain's elementary horizontal area times its water head ($A_O h_O$) accounts for q_{oc} being a flux per unit volume of overland flow domain. For submerged weir conditions, the flow is expressed as

$$\begin{aligned} q_{oc}^{submerged}A_O h_O &= C_d\frac{2}{3}\sqrt{2g}(2L_C)(h_u - h_d)^{1/2}(h_u - Z_{BANK}) \\ &= Q_{oc}^{submerged} \end{aligned} \tag{24}$$

which may also be expressed in terms of q_{oc}^{free}, the flux for a free flowing system, by manipulation of Eqs. (23) and (24) to give

$$q_{oc}^{submerged} = q_{oc}^{free}[(h_u - h_d)/(h_u - Z_{bank})]^{1/2} \tag{25}$$

where h_d is the downstream head between the two systems (h_d corresponds to h_C in Fig. 4). Eq. (23) or (25) is used for the interaction term, depending on overbank flow conditions, with q_{oc} equal to zero when h_u is below Z_{BANK}. Note that these flux relations are symmetric, and the same flow occurs from the overland flow surface to the channel segment for a given gradient, as would occur from the channel segment if the direction of the gradient were reversed.

2.6. Treatment of structures

Structures such as weirs, levees, gates, culverts, manholes, drop-structures, pump stations, and bridges may all be present within a channel reach, and require

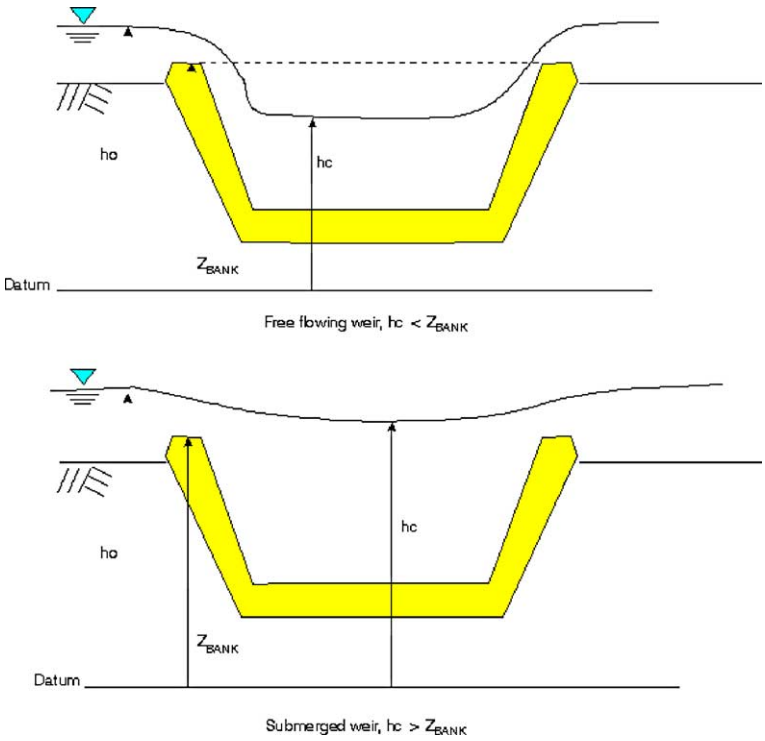

Fig. 4. Channel-overland flow interaction. Note: The figures show flow from the overland flow system (o) to the channel system (c). Similar considerations exist for flow from the channel to the overland flow system.

appropriate quantification to correctly depict a river or stream system that has been influenced by development. Each type of structure may have a number of different design types, shapes, sizes, or pipe configurations with different formulas governing the flow over/under/through each. Therefore, to accommodate various structures and designs in a general manner, their input is provided via tabular relations of various structure design flow conditions. A pre-processor may generate this tabular input via observed fluxes at a structure, or via flow-stage relations for the various designs of each structure.

Structures within a channel reach are accommodated into a model in a general manner if a Q vs h type of relationship for flow over the structure is known and can be prescribed by the user. The structure of type Q–h_{ups} allows for a symmetric flux value (Q) across the structure; this flux value is a function of the head value upstream to the structure (e.g., a free-flowing weir for which the flux across it is independent of which side is upstream). The structure of type Q–h_1h_2 is a more general relationship which allows for computation of flux (Q) across the structure as a function of the heads on both sides of the structure (e.g., a submerged weir/free-flowing weir). For the general upstream gradient relationships that may be generated for flow over a structure, the flux Q is positive when h_1 is greater than h_2, and vice versa,. The structure of type Q–h_uh_d defines a symmetric flux Q (positive from upstream to downstream) that is dependent on the upstream and downstream head values (h_u and h_d) where h_u is greater than or equal to h_d. This type of structure may be generalized by the Q–h_1h_2 structure; however, the structure type Q–h_uh_d provides a convenience of input, since the negative flux range (when h_2 is greater than h_1) is not explicitly required as input for structures with symmetric flux relationships. Yet another type of structure allows for input of Q_1–h_1 and Q_2–h_2 relations as non-symmetric fluxes that occur over the structure with net flow such that flow from 1 to 2 (Q_1) depends on h_1 and flow from 2 to 1 (Q_2) depends on h_2 (e.g., complex or gated systems or pumps).

When structures are present at a location, the second term of Eq. (13) which defines the flux between adjacent channel segments is replaced by the structure's flux relationship. Furthermore, when the flux across a structure depends on both head values straddling the structure, tabular input includes a 1-D vector for h_1 followed by another 1-D vector for $(h_1$–$h_2)$, followed by a 2-D matrix containing the corresponding flux values for each of the interpolation points. In this manner, Q may be entered as zero when $(h_1$–$h_2)$ is zero, for all tabulated values of h_1 (or h_{ups}). This consideration is important to ensure that the constraint $Q = 0$ when $h_1 = h_2$ can be maintained, for all interpolations generated from the table. Finally, a structure may be used as a link between any two nodes within the system to provide a flow connection between them. This can help to short-

circuit small-scale details, while still maintaining a flow connection between two locations. For instance, a neighborhood's drainage system details may be bypassed in large-scale simulations by providing a flow link between the neighborhood's overland flow grid block and a distant drainage outlet location; with the associated structure's tabulated relations representing the gross behavior of the drainage system.

Regulation of structures is common practice along many waterways and is simulated via a set of rules. Rules for operating structures include: specifying the time period during which specific rules apply to a structure; specifying the maximum flow rate through a structure (independent of the structure's stage-discharge relationships); specifying a trigger value of head/flux at any surface or subsurface location, above/below which a structure is opened/closed (two-way rules may also be provided); specifying a range of head/flux values above/below the trigger (as the case may be) over which the structure is linearly opened/closed (note that this range allows for smoothness in structure operation and should be set at a small value of around 10^{-6} m^{-1} for discrete open/close structure operations); specifying dependent (logical "AND" state) or independent (logical "OR" state) conditions between multiple rules for operating a structure; and specifying shift-work rules whereby structures are either kept shut, or not operated, when outside of the shift-work period. A rule for flow over a structure is applied as a multiplier k_{rRULE}, to the flow conditions of the structure. Thus, when $k_{\mathrm{rRULE}} = 1$, the associated structure is in a fully "on" state, while when $k_{\mathrm{rRULE}} = 0$, the associated structure is completely off. A partially open structure exists when water levels are within the prescribed range of the trigger value, that fully opens or closes the structure. The independent condition for opening a structure is provided by the maximum of all k_{rRULE} values between successive "OR" rules that operate a structure. The independent condition for closing a structure is provided by the minimum of all k_{rRULE} values between successive "OR" rules that operate a structure. The dependent condition for opening a structure is provided by a multiplication of all k_{rRULE} values between successive "AND" rules that operate a structure. The dependent condition for closing a structure is provided by a multiplication of all $(1 - k_{\mathrm{rRULE}})$ values between successive "AND" rules that operate a structure. This method of applying multiple rules provides a smoothness in the functions for operating a structure, thus precluding oscillatory non-convergence behavior.

2.7. Treatment of small surface-water bodies at large simulation scales

Conceptually, all surface-water bodies such as lakes, ponds, or wetlands may be treated by the two-dimensional overland flow equations by providing appropriate topography and bathymetry. However, this is not possible when the scale of the surface-water body is on the order of (or smaller than) its associated overland flow grid-block. Such features are effectively handled without over-discretization of the overland flow surface by assigning the appropriate channel node as a surface-water body. The surface-water body node thus has flow-connections along the channel dimension as well as to its appropriate overland flow node and subsurface node. A general tabulated relationship is then needed for a surface-water body node to describe its wetted area and volume characteristics, which are used in place of computations that use channel cross-sectional area and length. Specifically, tabulated values of surface area vs depth allow for the computation of storage volume as used by the first term of Eq. (13) and of the wetted area available for leakage to the subsurface (the term $L_C P_{\mathrm{ups}}$ in Eq. (19)). Also, overland/channel interactions occur over the perimeter of the surface-water body, which is prescribed for a surface-water body and is used instead of the $2\,L_C$ term in Eqs. (23) and (24). A surface-water body may additionally exhibit varying leakage to the subsurface, depending on its ponded depth. For this case, the term P in Eqs. (21) and (22) is replaced by the appropriate surface area of the surface-water body at its given depth (as interpolated from the tabular input), since this is now the area over which the surface-water body interacts with the subsurface. Along the dimension of the channels (l of Eq. (13)), the surface-water body may be connected to other channel nodes directly or via structures. A surface-water body node is, however, connected to another surface-water body node only via a structure which can govern flow between them (i.e., if two adjacent nodes of Eq. (13) are surface-water features, the flow term (second term) has to be defined by a structure). This 'pond routing' concept can again alleviate small-scale details via the use of structures.

2.8. Treatment of boundary conditions

Boundary conditions to the subsurface include prescribed head or flux conditions, well conditions, recharge, and general head boundaries. River or drain boundary conditions are also provided, if rigorous modeling of the river/channel system is not warranted. Surface-water boundary conditions also include prescribed head or flux conditions, and further include zero-depth-gradient and critical depth conditions. For the overland flow system, the discharge per unit width normal to the flow direction, Q_i (L^2T^{-1}), at the zero-depth gradient (ZDG) boundary is given by

$$Q_i = \frac{1}{n_i} d^{5/3} \sqrt{S_o} = C_i d^{3/2} \sqrt{S_o} = \sqrt{\frac{8g}{f_i}} d^{3/2} \sqrt{S_o} \qquad (26)$$

for the Manning equation, the Chezy equation and the Darcy–Weisbach relation respectively, where i is the direction of the zero-depth gradient discharge ($i = x$ in the x-direction and $i = y$ in the y-direction); and S_o is the bed slope (dimensionless) at the zero-depth gradient boundary. The critical depth (CD) condition forces the depth at the boundary to be equal to the critical depth, as would occur at free-fall boundaries. The discharge (Q_i) per unit width at the critical depth boundary is given by

$$Q_i = \sqrt{gd^3} \tag{27}$$

For a channel boundary, the total discharge, Q_C (L^3T^{-1}), at the zero-depth gradient boundary is given by

$$Q_C = \frac{1}{n_\ell}\frac{A^{5/3}}{P^{2/3}}\sqrt{S_o} = C_\ell \frac{A^{3/2}}{P^{1/2}}\sqrt{S_o} = \sqrt{\frac{8g}{f_\ell}}\frac{A^{3/2}}{P^{1/2}}\sqrt{S_o} \tag{28}$$

for the Manning equation, the Chezy equation and the Darcy–Weisbach relation respectively. The discharge, (Q_C) at critical depth conditions in a channel is given by

$$Q_C = \sqrt{\frac{gA^3}{B}} \tag{29}$$

A general outflow boundary condition (probably occurring over a structure) in a channel may also be provided by user-defined, tabulated Q–h relations at a channel outflow boundary.

2.9. Treatment of interception and evapotranspiration

Interception and comprehensive evapotranspiration are simulated as mechanistic processes governed by plant and climatic conditions as noted by Kristensen and Jensen [22], and Wigmosta et al. [44]. Interception is the process involving retention of a certain amount of precipitation on the leaves, branches, and stems of vegetation or on buildings and structures in urban areas. The interception process is simulated by the bucket model, wherein precipitation in excess of interception storage and evaporation from interception reaches the ground surface. This is efficiently computed at the start of every time step of simulation, by keeping track of S_{int}, the interception storage (L), for each areal model location. The interception storage varies between zero and S_{int}^{max}, the interception storage capacity (L), which depends on the vegetation type and its stage of development. It is calculated from [22]

$$S_{int}^{max} = c_{int}\mathrm{LAI} \tag{30}$$

where LAI is the dimensionless leaf area index; and c_{int} is the canopy storage parameter (L). Note that LAI represents the cover of leaves over a unit area of the ground surface, and may be prescribed in a time-dependent manner. The interception storage is filled by rainfall and depleted by evaporation. For each time increment Δt, the actual interception storage (S_{int}) is calculated as follows:

$$S_{int}^{*} = \min(S_{int}^{max}, S_{int}^{0} + P_P\Delta t) \tag{31}$$

with

$$E_{can}\Delta t = \min(S_{int}^{*}, E_p\Delta t) \tag{32}$$

and

$$S_{int} = S_{int}^{*} - E_{can}\Delta t \tag{33}$$

where S_{int}^{0} and S_{int}^{*} are the previous-time and intermediate values of S_{int}, respectively; P_P is the precipitation rate (LT^{-1}); E_{can} is the canopy evaporation (LT^{-1}); and E_p is the reference evapotranspiration (LT^{-1}), which may be derived from pan measurements or computed from vegetation and climatic factors (radiation, wind, humidity and temperature) using the Penman–Monteith equation [25] for vegetated surfaces or a bare-ground evaporation formula [32] for non-vegetated surfaces, as a function of temperature, wind and humidity conditions. The reference evapotranspiration is computed efficiently at the start of a simulation, for further use in determining the actual evapotranspiration. The reduced rainfall rate ($\hat{P}_P$) which reaches ground surface after interception is given by

$$\hat{P}_P = P_P - (S_{int} - S_{int}^{0})/\Delta t - E_{can} \geqslant 0 \tag{34}$$

Similarly, the potential for evapotranspiration from the soil surface and below is reduced by the canopy evapotranspiration term, which is carried through in the subsequent discussions.

Evapotranspiration is rigorously modeled as a combination of plant transpiration and of evaporation, and affects nodes in both surface and subsurface flow domains. Transpiration from vegetation occurs within the root zone of the subsurface which may be above or below the water table and may involve several nodal layers. The rate of transpiration for node I (T_{pI}) is estimated using the following relationship that distributes the net capacity for transpiration among various factors [22]:

$$T_{pI} = [f_1(\mathrm{LAI})][f_2(\theta_I)][RDF_I][E_p - E_{can}] \tag{35}$$

where f_1 (LAI) is a function of leaf area index (dimensionless); $f_2(\theta_I)$ is a function of nodal water content (dimensionless); and RDF_I is the nodal value of the root distribution function (dimensionless) which may be prescribed in a time-varying manner. The vegetation term is expressed as

$$f_1(\mathrm{LAI}) = \max\{0, \min[1, (C_2 + C_1\mathrm{LAI})]\} \tag{36}$$

The root zone term is defined by the relationship:

$$\mathrm{RDF}_\mathrm{I} = \int_{z_1}^{z_2} r_\mathrm{F}(z)\,\mathrm{d}z \Big/ \int_0^{L_1} r_\mathrm{F}(z)\,\mathrm{d}z \tag{37}$$

and the moisture content dependence term is expressed as

$$f_2(\theta_\mathrm{I}) = \begin{cases} 0 & \text{for } 0 \leqslant \theta_\mathrm{I} \leqslant \theta_\mathrm{wp} \\ 1 - \left[\frac{\theta_\mathrm{fc}-\theta_\mathrm{I}}{\theta_\mathrm{fc}-\theta_\mathrm{wp}}\right]^{c_3/E_\mathrm{P}} & \text{for } \theta_\mathrm{wp} < \theta_\mathrm{I} \leqslant \theta_\mathrm{fc} \\ 1 & \text{for } \theta_\mathrm{fc} < \theta_\mathrm{I} \leqslant \theta_0 \\ \left[\frac{\theta_\mathrm{an}-\theta_\mathrm{I}}{\theta_\mathrm{an}-\theta_0}\right]^{c_3/E_\mathrm{p}} & \text{for } \theta_0 < \theta_\mathrm{I} \leqslant \theta_\mathrm{an} \\ 0 & \text{for } \theta_\mathrm{an} \leqslant \theta_\mathrm{I} \end{cases} \tag{38}$$

where C_1, C_2 and C_3/E_p are dimensionless fitting parameters; L_r is the effective root length; z is the depth coordinate from the soil surface; θ_fc, θ_wp, θ_o and θ_an are the moisture contents at field capacity, wilting point, oxic limit and anoxic limit respectively; and $r_\mathrm{F}(z)$ is the root extraction function which typically varies logarithmically with depth. The function f_1 correlates the transpiration from a node (T_PI) with the leaf area index (LAI) in a linear fashion. The function f_2 correlates T_PI with the moisture state of the node containing the roots and is an extension of the function of Kristensen and Jensen [22] to account for root processes in greater detail. Below the wilting-point moisture content, transpiration is zero; transpiration then increases to a maximum at the field-capacity moisture content. This maximum is maintained up to the oxic moisture content, beyond which the transpiration decreases to zero at the anoxic moisture content. When available moisture is larger than the anoxic moisture content, the roots become inactive due to lack of aeration [10]. In general, $f_2(\theta_\mathrm{I})$ is a nonlinear function of θ_I, though the ramping function is linear when $C_3/E_\mathrm{p} = 1$. Values of RDF_I should be prescribed such that the following constraint holds among each vertical set of nodes at any time:

$$\mathrm{RDF} = \sum_{I=1}^{n_\mathrm{R}} \mathrm{RDF}_\mathrm{I} = 1 \tag{39}$$

where n_R is the number of nodes that contribute to the total root zone for each areal location; and Eq. (39) is obtained by expressing Eq. (37) over the discretized layers of nodes containing the roots. As a practical matter, however, the value of RDF at any areal location may be less than one to account for ineffective roots. For each time step, the transpiration (T_p) over the effective root length is calculated as the sum of the transpiration from each of the nodes at depth, as

$$T_\mathrm{p} = \sum_{I=1}^{n_\mathrm{R}} T_\mathrm{pI} \tag{40}$$

where n_R is the number nodes that lie within the depth interval $0 \leqslant z \leqslant L_\mathrm{R}$, at any areal location.

Two models are provided for evaporation. The first model assumes that evaporation occurs if the reference evapotranspiration has not been removed by the above processes of canopy evaporation and plant transpiration. Therefore, evaporation from the soil surface and subsurface soil layers is estimated as follows:

$$E_{\mathrm{s_I}} = [\alpha_\mathrm{I}^*][E_\mathrm{p} - E_\mathrm{can} - T_\mathrm{p}][\mathrm{EDF}_\mathrm{I}] \tag{41}$$

The second model assumes that evaporation occurs along with transpiration, resulting from energy that penetrates the vegetation cover and is expressed as

$$E_{\mathrm{s_I}} = [\alpha_\mathrm{I}^*][E_\mathrm{p} - E_\mathrm{can}][1 - f_1(\mathrm{LAI})][\mathrm{EDF}_\mathrm{I}] \tag{42}$$

where α_I^* is the wetness factor given by

$$\alpha_\mathrm{I}^* = \begin{cases} (\theta_\mathrm{I} - \theta_{e2})/(\theta_{e1} - \theta_{e2}) & \text{for } \theta_{e2} \leqslant \theta \leqslant \theta_{e1} \\ 1 & \text{for } \theta_\mathrm{I} > \theta_{e1} \\ 0 & \text{for } \theta_\mathrm{I} < \theta_{e2} \end{cases} \tag{43}$$

where θ_{e1} is the moisture content at the end of the energy-limiting stage (above which full evaporation can occur), and θ_{e2} is the limiting moisture content below which evaporation is zero [2]. Eq. (43) expresses the moisture availability term for the subsurface domain. For the overland flow domain, α_I^* is calculated as varying between unity when the elevation of flow is at or above depression storage ($\mathrm{LS} + h_\mathrm{ds}$) and zero for a flow elevation at the land surface (LS), thus representing the reduced evaporative area of available water on the overland flow node within the depressions.

The term EDF_I in Eq. (41) or (42) is the evaporation distribution function among a vertical set of nodes that includes the overland and subsurface flow domains. Two alternate conceptualizations are provided for EDF_I. For the first model, it is assumed that the capacity for evaporation ($[E_\mathrm{p} - E_\mathrm{can} - T_\mathrm{p}]$ in Eq. (41) or $[(E_\mathrm{p} - E_\mathrm{can})(1 - f_1(\mathrm{LAI}))]$ in Eq. (42)) decreases with depth below the surface (subject to available moisture) due to the reduction of energy penetration in the soil. Therefore, an appropriate EDF_I for each cell layer may be prescribed as a function of its depth from land surface. For the second model, the capacity for evaporation is met from the land surface downward to a prescribed extinction depth (B_soil).

3. Numerical solution

3.1. Domain discretization

The system of equations governing moisture movement through the hydrologic cycle have been discussed above. The spatial domains include the subsurface domain, the overland flow domain, and the channel flow domain. The subsurface domain is discretized using a block-centered finite-difference scheme, based on the framework of the popular groundwater flow model, MODFLOW [24]. The subsurface grid may be distorted vertically to reflect hydrostratigraphic boundaries and

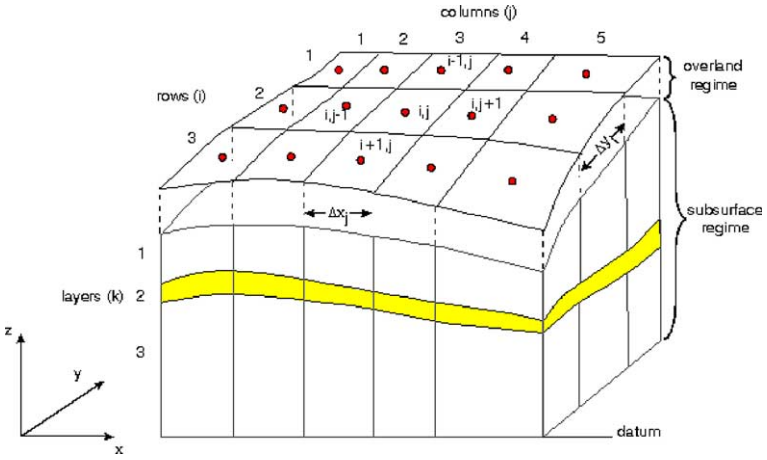

Fig. 5. Spatial discretization of the subsurface and overland flow surface.

may be orthogonal-curvilinear in its areal dimensions to follow complex boundaries or flow-lines. The overland flow domain grid areally mirrors the subsurface grid as shown in Fig. 5, with overland flow node elevations corresponding to the land surface elevation. The channel flow domain is discretized using a finite volume concept with the channel network superimposed on the overland flow and subsurface domains as shown in Fig. 6. The channel regime discretization is completely independent of the areal grids, and there are no constraints on discretizing the channel network that arise from discretization considerations given to the subsurface or overland flow regimes. Further, the channel segments may be discretized in any order due to the general nature of the equations and solution schemes. The solution methods discussed here do not require upstream to downstream numbering conventions for reaches or junctions as needed by several other methods. Special numbering schemes complicate input of information using automated GIS tools and assume a priori upstream and downstream directions. For the scheme used in this study, the upstream and downstream locations are governed by the flow system that develops, and it is therefore of more general applicability.

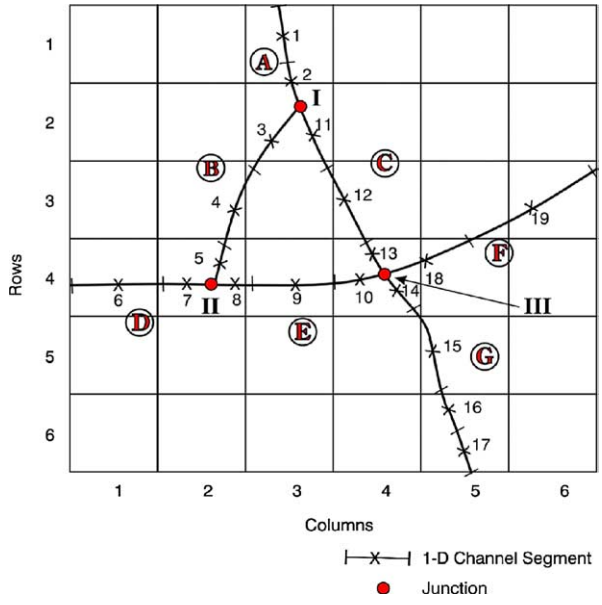

Fig. 6. Discretization of channel networks on a subsurface grid.

The channel network consists of interconnected reaches, each of which is divided into sequentially numbered segments with nodes at their centers. For flexibility, several channel segments may be connected to a single node of the subsurface or overland flow domain grid (e.g., channel segments 16 and 17 both lie in row 6, column 5 as depicted in Fig. 6) or a channel segments may span several nodes of the areal grid (e.g., channel segment 19 spans columns 5 and 6 in row 3 as depicted in Fig. 6). Junctions are defined as channel intersections (e.g., Junction III connects channel segments 10, 13, 14, and 18 of reaches C, E, F, and G, as depicted in Fig. 6). A channel segment may alternatively be used to depict a surface-water body, and flow between two adjacent segments may be controlled by a hydraulic structure. The one-dimensional segments may also be connected to deeper subsurface layers to model subsurface pipes and drainage systems. The discretized set of governing equations (13) are applied to flow between any two connecting cells along a reach, then to all connecting cells (two at a time) at junctions. Structure flux relations replace the flow terms, and, where present, surface-water features replace the storage terms and terms for quantifying flow across domains.

3.2. Coupling, time-stepping and other solution considerations

Eqs. (1), (6) and (13) govern flow of water within and among all flow regimes. The discretized system is solved

by a fully implicit time-marching procedure, when the interaction fluxes as provided by Eqs. (18), (19), (23) and (25) are substituted into the governing flow equations. Alternatively, the subsurface flow equations may be linked (in a time-lagged manner) or iteratively coupled to a simultaneous solution to the overland and channel flow equations. Two alternatives are provided for linking/iterative coupling. For the first option, the linking fluxes as provided by Eqs. (18) and (19) are directly applied to each domain as a boundary condition. For the second option, the surface-water heads are used as a general head boundary for solving the subsurface equations, and the subsurface heads are used as a general head boundary for solving the surface-water equations. This linking/iterative coupling approach requires that a small depression storage (10^{-6} m^{-1}) be allowed so that the k_{rgo} and k_{rgc} term of Eqs. (18) and (19) approach zero in a smooth manner. Linking approaches used by others [1,26,34] check the rainfall only against the infiltration capacity, thus neglecting that the overland flow component that is generated in one area can infiltrate in other areas. Fiedler and Ramirez [12] include this term in their linking scheme by examining all incoming flows. Convergence for the iteratively coupled approach is obtained when the absolute or relative flux between domains changes within prescribed tolerance limits from that of the previous iteration. Convergence for the fully implicit method, or for each of the domains of the linked/iteratively coupled approach, is obtained when the change in head values in the respective domains are within prescribed tolerance limits. Fully implicit discretization is the most robust and efficient solution scheme for the coupled system of surface/subsurface flow equations and is theoretically most correct. However, linked/iteratively coupled approaches allow for providing different time scales to the surface and the subsurface flows, and several small surface-water flow time steps may be solved for each large subsurface time-step solution. Linked/iteratively coupled approaches are therefore useful when surface/subsurface interactions are small. Further, when all options are available, the validity and accuracy of the linked approach may be tested before accepting/rejecting it as a feasible or more efficient alternative for solving complex systems.

The modified Picard scheme as discussed by Celia et al. [5] or the Newton–Raphson procedure with under-relaxation as detailed by Huyakorn and Pinder [20] and Huyakorn et al. [21] is used to linearize the subsurface flow equation, and similar methods are followed for linearizing the surface-water flow equations for both fully coupled and linked approaches. The boundary conditions of Eqs. (26)–(29) are always applied with Newton–Raphson linearization because they appear only on the diagonal and do not destroy matrix symmetry for the modified Picard scheme. All sink conditions are applied with the physical constraint that $Q = 0$ when no water is available. Thus, a sink strength decreases rapidly to zero at the limiting condition, and a Newton–Raphson linearization is applied to this function. The evapotranspiration formulation is also expanded in a Newton–Raphson fashion; however, this is assembled for all nodal layers within the root zone and the evaporative surface simultaneously, since the various evapotranspiration formulations have connectivities between all nodes of these zones. These connectivities may be established for the matrix prior to beginning the simulation, or they may be neglected (only adjacent connectivities are maintained, as per the flow equation) with Newton–Raphson linearization applied only to the immediate connectivities of a node (or only to the diagonal term for the case of a modified Picard solution). It should be noted that the evaporation model of Eq. (42) along with the first model for $\mathrm{EDF_I}$ only generates diagonal terms; therefore, the full Newton–Raphson scheme may be applied even for a modified Picard linearization scheme. The unsymmetric matrix equations generated at each non-linear iteration are solved using the Orthomin scheme detailed by Panday et al. [27].

Adaptive time-stepping is provided such that the time-step size grows (up to a maximum) when the number of iterations required for convergence is low (solution is easy); reduces when the number of iterations is high; and is considered optimal with no change when the number of iterations required for convergence to a previous time-step is medium as compared to the prescribed maximum number of iterations [19]. For linked/iteratively coupled solutions, the surface-water domain solution is also adaptive in time, where its time-step size is governed by the ease with which the surface-water domain is solved. However, this time-step size cannot be larger than the current time-step size used for the subsurface domain, which is governed by the ease with which the subsurface equations are solved. Additionally, for iteratively coupled schemes, the time-step size used for the subsurface domain is also governed by the ease with which the iterative coupling procedure converges.

The procedures discussed here constitute a current state-of-the-art solution to the set of governing equations for surface or subsurface flow and are detailed in the referenced publications. Therefore, the discussions that follow focus on special considerations provided to efficiently solve the conjunctive water flow problem in real-world situations at various scales.

3.3. Treatment of the surface-water flow conductance terms

Careful consideration should be provided to numerical implementation of the conductances within the flow term of Eqs. (6) and (13). The flow coefficients k_x and k_y of Eq. (6) and κ_ℓ of Eq. (13) are combinations of the

properties of the two nodes involved in the respective flow connection, as provided by Eqs. (7), (8) and (14). The frictional resistance (or roughness term) between two nodes in Eqs. (7) and (8) is a constant ($1/n_x$ and $1/n_y$ for Manning, C_x and C_y for Chezy, or $\sqrt{8g/f_x}$ and $\sqrt{8g/f_y}$ for Darcy–Weisbach, all referred to as H_x and H_y) and is computed as the weighted harmonic mean of the values of the two communicating cells, weighted by the flow lengths of each of the cells for a rectangular grid. Thus

$$H_{xj,j+1} = \frac{H_{xj}H_{xj+1}(\Delta x_j + \Delta x_{j+1})}{(H_{xj}\Delta x_{j+1} + H_{xj+1}\Delta x_j)} \tag{44}$$

and

$$H_{yi,i+1} = \frac{H_{yi}H_{yi+1}(\Delta y_i + \Delta y_{i+1})}{(H_{yi}\Delta y_{i+1} + H_{yi+1}\Delta y_i)} \tag{45}$$

For a curvilinear geometry, the harmonic mean is weighted by the respective cell areas. Similarly, the roughness term in Eq. (14) for channel flow may be expressed by the harmonic mean of the individual cells weighted by their respective wetted areas. Use of a weighted harmonic mean for the roughness term is consistent with use of a weighted harmonic mean to represent the absolute hydraulic conductivity value between two adjacent groundwater flow cells, providing a bias toward the lower conductivity value for controlling flow. Additionally, if the friction factors are computed for the Darcy–Weisbach relation using Eqs. (10)–(12) during the course of a simulation, with the velocity term computed by using the previous iteration head values in the calculation of Reynolds number. Therefore, the Darcy–Weisbach relation has the potential of being numerically weaker than the other friction relations.

The gradient part of Eqs. (7) and (8) ($[\partial h/\partial s]^{-1/2}$) is calculated from the average x- and y-direction gradients of the connecting cells to determine the gradient in the direction of maximum slope. This term is not expanded as per Newton–Raphson linearization—its previous iteration value is used instead. This is because a cross-connection term is involved, and extra connectivities will need to be generated to incorporate its full Newton expansion into the finite-difference solution scheme. Further, the slope of this term is infinite when the water level is flat (zero head gradients) causing instabilities in the matrix solver and in the Newton procedure. Similarly, the gradient term in Eq. (14) for channel flow ($[\mathrm{d}h/\mathrm{d}\ell]^{-1/2}$) is calculated from the flow gradient between the two connecting cells i and j. This term is not expanded as per Newton–Raphson linearization because its slope is infinite when the water level is flat; this causes numerical instabilities, as discussed above. Further, this term is limited to a maximum value of 10^{10} for numerical considerations.

The remaining terms in Eqs. (7) and (8) for overland flow, along with the depth within the first gradient operator of Eq. (6), combine to $d^{5/3}$ for Manning, $d^{3/2}$ for Chezy and $d^{3/2}$ for the Darcy–Weisbach relation. In a similar manner, remaining terms in Eq. (14) for channel flow are $[A^{5/3}/(P^{2/3})]$ for Manning, $[A^{3/2}/(P^{1/2})]$ for Chezy and $[A^{3/2}/(P^{1/2})]$ for the Darcy–Weisbach relation, which are a function of depth of flow within the channel section. These depths are computed from above the depression storage elevations ($\mathrm{LS} + h_{\mathrm{ds}}$) as discussed earlier in Section 2.4 to account for unevenness at the grid scale (note that the depths involved in the storage term of Eqs. (6) and (13) begin at LS and include variable porosity as defined by the "volumetric head" up to ($\mathrm{LS} + h_{\mathrm{ds}} + h_{\mathrm{os}}$) to quantify the effects of depressions and obstructions). Full upstream weighting of this term between the two connecting nodes ensures a monotonic solution, in a parallel manner to k_{r} in the subsurface flow equation. This is because upstream weighting ensures that flow from a dry node is zero, maintaining the physical reality in the set of governing equations.

An alternative formulation is also provided to calculate depth in the flow-depth term. According to standard procedures, this depth is calculated as water elevation at a node, minus the surface elevation for that node (specifically, $d_i = h_i - [(\mathrm{LS} + h_{\mathrm{ds}})_i]$ for node i). The alternate formulation considers the two nodes between which flow occurs and computes the depth for flow at the nodes using the sill elevation at the interface between the two nodes i and j. Thus

$$d_i = h_i - \mathrm{sill}_{ij} \tag{46}$$

and

$$d_j = h_j - \mathrm{sill}_{ij} \tag{47}$$

where

$$\mathrm{sill}_{ij} = \max[(\mathrm{LS} + h_{\mathrm{ds}})_i, (\mathrm{LS} + h_{\mathrm{ds}})_j] \tag{48}$$

This is a more natural expression of the depth of flow between two nodes of the discretized system because the conductance term for a node becomes non-zero only when its water level is above the sill to the connecting node, as in the case of flow over a weir or over channel banks. The new expressions further alleviate convergence difficulties in computing overland flow, for cases where water flows from a node at a lower elevation to a node at a higher elevation, as in the filling of a pond. When the node at the higher elevation is dry, with water level at the adjacent (lower) node below its sill, the higher (dry) node is the upstream node. Thus, no water flows between the two nodes since the upstream depth in the flow term is zero. However, when the water level at the lower node rises above the sill, the lower node switches to become the upstream node. In this case, the conductance term for flow onto the dry node activates in a gradual manner with the new formulation. In contrast, use of the standard method could result in an extremely high initial estimate being chosen for the conductance

term, thus hindering convergence. A central weighting approximation may also be used by either the standard or the alternate procedures for calculating the relative conductance terms as may be done for the relative permeability term (k_r) in the subsurface flow equation. It should be noted that the use of central weighting with the alternate scheme for the surface-water flow equations also provides correct solutions with zero flow occurring from a dry node. Independent control is therefore useful for either upstream or central weighting solution options for the subsurface and surface-water flow equations.

4. Verification examples

4.1. General

The processes and schemes discussed above have been implemented into MODHMS [19] which is a MODFLOW-based modeling system for surface/subsurface simulations of the water budget. Extensive testing was performed at every stage of development including spot-checking the terms of the matrix and right-hand side vector against manual calculations for code design problems. The code was then benchmarked against a series of published analytical solutions for each of the domains, compared with other numerical solutions for single-domain and conjunctive applications, and applied to perform field-scale simulations. These benchmark tests have been documented by HydroGeoLogic [19], and their results compare well with the complimentary solutions.

The examples discussed here concern various aspects of flow behavior discussed in the theory, in a systematic manner. Lessons learned from the step-by-step approach of simplified problems are valuable for simulations of complex field systems.

4.2. Surface-water flow over a tilted V-catchment

This problem considers two-dimensional overland flow on a tilted V-catchment (Fig. 7) generated by a rainfall event as simulated by diGiammarco et al. [8] and VanderKwaak [39]. Only one half of the domain is simulated due to symmetry, with the simulated outflow discharge doubled to produce equivalent results. The simulation domain therefore consists of a 1000 m × 800 m slope connected to a 1000 m length of channel 10 m wide. Surface slopes are 0.05 and 0.02 perpendicular to and parallel to the channel respectively. Mannings roughness coefficients of 0.015 and 0.15 are applied to the slope and channel, respectively. Although unrealistic in natural conditions, these Manning's values were used to facilitate comparison with other available solutions. Simulations are conducted with critical depth and zero-depth gradient boundary conditions at the downstream end of the channel. Simulation results are also compared with those from two traditional hydrologic simulation models, HSPF and HEC-1. HSPF [3] is a continuous watershed simulation model based on the original Stanford Watershed Model IV developed by Crawford and Linsely [7]. Note that the HSPF model cannot accommodate zero depth gradient boundaries and therefore a critical depth condition is used for the comparison simulations. The HEC-1 model, developed by the USACE [37] Hydrologic Engineering Center, California, cannot handle critical depth boundaries. Therefore, a zero depth gradient condition was specified as the downgradient boundary condition with HEC-1.

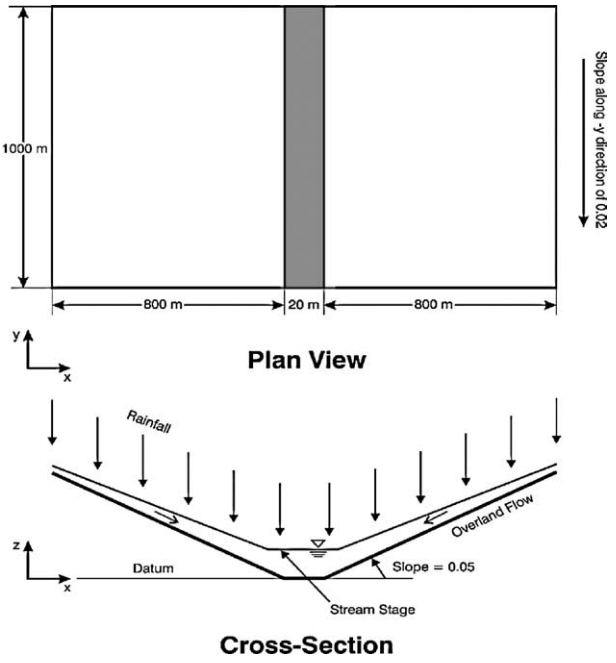

Fig. 7. Schematic description of tilted V-catchment flow problem.

The domain is discretized into 16 rows and 20 columns of overland flow nodes and one reach of channel flow nodes. The areal grid dimensions are 50 m × 50 m for the overland flow domain with a rectangular channel cross-section of length 50 m and width 10 m discretizing the channel flow domain. Rainfall at the rate of 3×10^{-6} m/s is applied on the surface for 90 min, with zero rainfall for the next 90 min of simulation as discussed by diGiammarco et al. [8]. Adaptive time stepping is provided with an initial time-step size of 5 s, a maximum time-step size of 100 s, and a time-step incrementing factor of 2.0. The system of surface-water flow equations is solved using Newton–Raphson linearization, with 100 and 15 maximum inner and outer iterations, respectively and a convergence tolerance of 10^{-3} m. Fig. 8 compares the predicted discharge using the current model with critical depth and zero-depth gradient boundary conditions to predictions from the other codes. The outflow

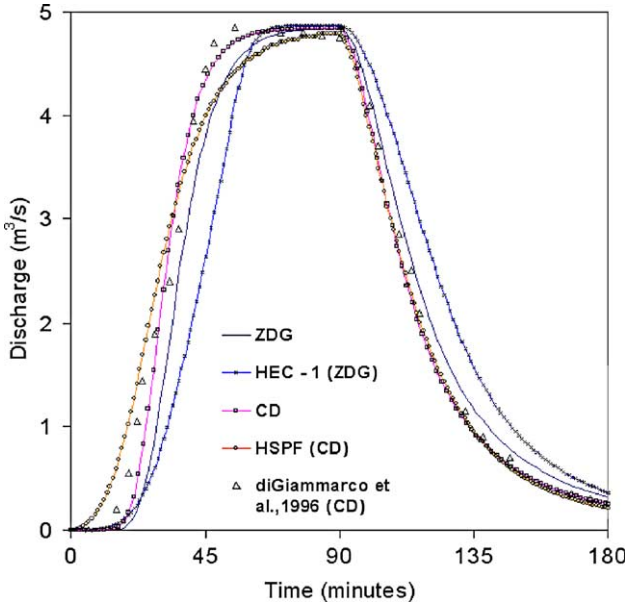

Fig. 8. Outflow hydrograph for various simulations of the V-catchment problem (ZDG = zero depth gradient boundary; CD = critical depth boundary).

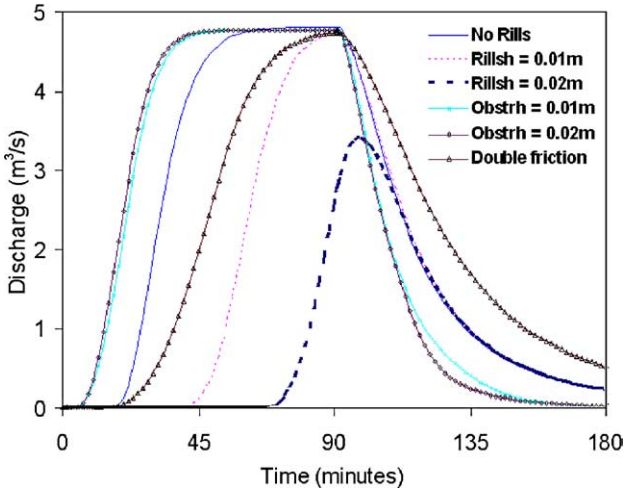

Fig. 9. Sensitivity of outflow hydrograph to various parameters for the V-catchment Problem (Rillsh = height of depression storage; Obstrh = height of obstruction storage exclusion).

hydrograph predicted by HSPF and the critical depth condition simulation show excellent agreement for the peak flow discharge and the receding limb of the hydrograph. However, there is a discrepancy on the rising limb of the hydrograph where HSPF predicts the time to initial discharge to be slightly less than that predicted by the current model. Despite this disparity, the time to peak discharge is equal. The solution with critical-depth conditions matches well with that of diGiammarco et al. [8] for the entire hydrograph. A comparison of the zero-depth gradient simulation with the HEC-1 code shows fair agreement. There is a slight discrepancy on both the rising and receding limbs of the hydrograph, such that HEC-1 under-predicts discharge at early time and over-predicts discharge at late times relative to the current simulation. Most time-steps converged within two iterations for both simulations using the current formulation, with negligible mass balance errors at all time steps, thus verifying the overland flow and channel flow formulations and their interaction via weir type equations.

The sensitivity of the discharge hydrograph to various overland flow parameters is shown in Fig. 9. The presence of depressions delays the rising limb of the hydrograph, but does not affect the receding limb as compared to the base case with no depressions. The volume of water that occupies the depressions is unavailable to flow, thus the area under the hydrograph diminishes for increasing depression storage height. The presence of obstructions excludes storage at lower flow-depths, causing water to arrive earlier at the outlet, even though the obstruction heights add further resistance to flow at low flow depths. The receding limb is also earlier for higher obstruction heights and more so at lower flow depths due to smaller storage as well as lower conductances as compared to the base case. Doubling the Manning's friction coefficient causes a delay in both rising and receding limbs of the hydrograph. The peak discharge rate is the same for all cases (equal to the rainfall rate times total area) for fully developed flow on the overland and channel domains.

4.3. Surface/subsurface flow in a V-catchment basin

The tilted V-catchment example discussed in the preceding section is extended for this example to include the subsurface domain. The underlying aquifer extends to a depth of 20 m below the channel outlet location. No flow boundaries are applied along the aquifer lateral boundaries to enable analytical examination of the sub-watershed without additional complicating influences. The homogeneous subsurface is fully connected with the surficial layers (i.e., no skin layer effects) and is provided with sandy-loam material properties: horizontal and vertical hydraulic conductivity values of 5×10^{-5} and 5×10^{-6} m/s respectively, a porosity value of 0.1, and van Genuchten parameters as follows: $\alpha = 2.25\ \mathrm{m}^{-1}$, $\beta = 1.89$, and $S_{wr} = 0.16$. The domain is discretized into 11 subsurface layers with areal gridding mirroring the grid of the overland flow domain discussed earlier. The top ten subsurface layers each have a thickness of 1 m and the bottom of the last layer resides at $z = -20$ m (the channel outlet occurs at $z = 0$ m). The same rainfall intensity of 3×10^{-6} m/s as for the previous case is applied, such that the discharge at the outlet is 4.8 m^3/s for fully-developed overland flow. The base case simulation is performed for 35 days with the prescribed rainfall, with 15 more days of recession. Fig. 10 shows the out-

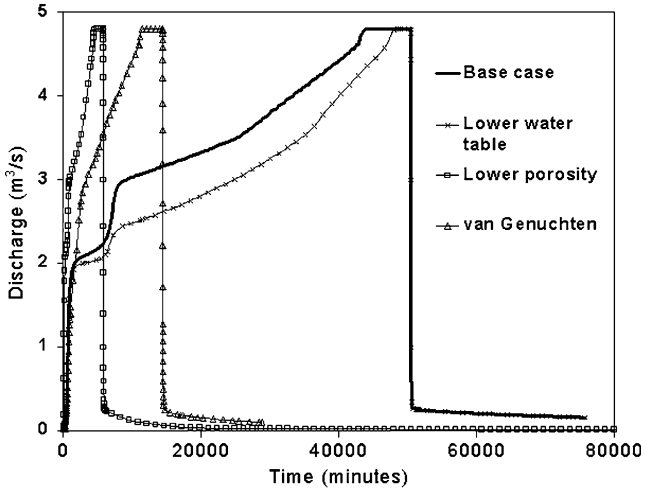

Fig. 10. Sensitivity of outflow hydrograph to various parameters for the conjunctive surface/subsurface flow problem.

flow hydrograph for this base case, and for three other sensitivity cases. The outflow hydrograph is noted to be more complex than the previous study of section 4.2 due to subsurface interactions, with the rising limb occurring at a much slower rate than for overland flow alone. The receding limb shows a distinct break between the overland runoff component and the baseflow component which continues for a longer period at a slower and more gradually declining rate. For the first sensitivity simulation, the starting water-table elevation is changed from 0 to −5 m. The outflow hydrograph for this case is a delayed replica of the base case hydrograph due to the additional pore-spaces that are filled before the surface gets saturated such that runoff occurs. For the second sensitivity case, the porosity is reduced an order of magnitude, and the rainfall event is prescribed as occurring for 4 days with 100 days of recession, since saturation excess conditions occur early. For this sensitivity case, the outflow hydrograph peaks in one-tenth the time as for the base case—the entire rising limb is in fact scaled down in time by a factor of 10. The baseflow portion of the receding limb drops quicker for this case, as the subsurface flow system rapidly approaches steady-state conditions resulting from lower porosities. The next sensitivity shows the effects of changing the van Genuchten parameters, to those of a more silty clay loam, with $\alpha = 0.25\ \mathrm{m}^{-1}$, $\beta = 1.35$, and $S_{wr} = 0.26$. Since moisture retention is greater for this case, the pores are filled quicker; this also results in a quicker peak for the discharge hydrograph. Thus, this case is investigated for a rainfall event of only 10 days, with an additional recession period of 10 days. The subsurface domain shows poorer convergence for this case, requiring on average, four times as much CPU time per day of simulation as for the base case. This computational difficulty results from the extremely non-linear van Genuchten relative permeability curve obtained with $\beta = 1.35$, exhibiting a large slope when saturation is almost unity. This computational burden is slightly alleviated by use of an equivalent Brooks–Corey function as defined by Eq. (4), with almost identical results (this case runs about three times slower per day of simulation than the base case).

Simulations are also performed using the decoupled approach for the base case problem. The first case involves a time-lagged head coupling between the two domains, with use of the same time-stepping as for the base case (TMAX = 4800 s for rainfall period and TMAX = 9600 s for recession period). The second case is similar to the first, with use of a much smaller maximum time-step size (200 s). The third and fourth cases follow the first two, but allow for iterations on the linked domains. A maximum of 21 iterations is allowed between domains. Fig. 11 shows the discharge hydrograph for the various cases. As may be noted, the decoupled approach gives similar results to the fully-coupled approach when the time-step size is sufficiently small, and the iterative solution provides an exact match with the fully-coupled solution. With the use of larger time-steps, however, the decoupled approaches give incorrect solutions for the rising limb of the hydrograph, even for the iterative scheme. Iterations between domains converge easily for the large time-step size of 4800 s; therefore, time-step cutting does not occur (which would make the solution more accurate) with a convergence tolerance limit for the interaction flux at 0.1%. The large time-step decoupled simulations exhibit mass balance errors of up to 30% during simulation of the rising limb. This indicates that the iteratively coupled scheme has not converged, even when heads and fluxes are within reasonable tolerance limits, highlighting the need to check that residuals are negligible to ensure

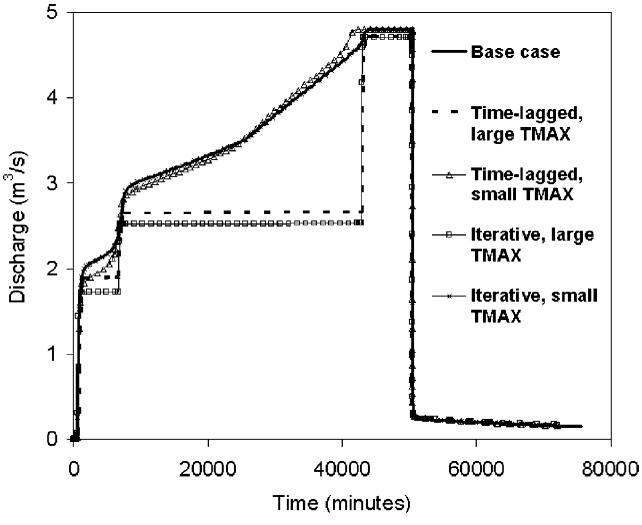

Fig. 11. Comparison of outflow hydrographs for fully coupled and head coupled solution schemes (small TMAX = 200 s; large TMAX = 4800 s).

correct solution convergence before proceeding with a new time step. Simulation times for the four cases are 0.96, 16, 3.4, and 58 times larger than that of the base case, respectively. Surface-water simulations do not take sub-time steps for any of these simulations, indicating that the surface-water flow solution is easy and that the interaction fluxes between domains is the determining factor for accuracy of results. Finally, it should be noted that use of flux-coupled solutions (as opposed to head-coupled solutions discussed here) fail in the subsurface domain for this problem, for both time-lagged and iterative methods using the large and small time-step sizes discussed above.

A final set of simulations is conducted to gauge the performance of the evapotranspiration formulation, for the same problem. The base case simulation is therefore supplemented with evapotranspiration losses as parameterized in Table 1. The evaporation model of equation (42) along with the first model for EDF_I (whereby EDF_I is prescribed as a capacity for evaporation decreasing with depth) are selected for this problem. Therefore, all terms of the hydrologic cycle are activated for this simulation, and the various water budget components are analyzed. Fig. 12 shows the outlet discharge rate, the net infiltration rate, the net exfiltration rate, and total evapotranspiration rate vs time for this simulation. The discharge hydrograph in Fig. 12 is unnoticeably slower than for the base case shown in Fig. 11 because evapotranspiration is only a small component (about 1%) of the total flow. Furthermore, the complexity of the discharge hydrograph shown in Fig. 11 is also explained by the additional components included in Fig. 12. Discharge at the outlet begins to occur at about 500 min and increases rapidly till about 1000 min. The corresponding infiltration rate curve drops rapidly until about 1000 min, at which point the slope of both curves becomes more gradual. The discharge curve becomes steeper at about 7500 min, corresponding with a steep rise in the groundwater exfiltration curve. The infiltration curve further drops at this stage because less area is available for infiltration as the lower portions of the V-catchment slope become saturated. Both exfiltration and discharge curves increase at a more gradual pace after around 9000 min. The infiltration curve reaches its saturated infiltration capacity at around 43,000 min and remains there until the end of the rainfall event. The evapotranspiration curve exhibits an interesting behavior, even though evapotranspiration rates are small and do not significantly affect the other components of the water budget shown in the figure. As each of the subsurface layers becomes wet due to infiltration, the evapotranspiration rate first increases and then decreases rapidly as that layer becomes saturated above its anoxic moisture content. This process is repeated as each of the first four layers (which contain the root zone) become saturated. At the start of the recession period, the evapotranspiration rate rapidly increases as water redistribution in the top layers of the subsurface reduce saturations below the oxic water limit. Continual drainage further reduces water contents to near wilting point levels, thus reducing the rates after about 55,500 min. Fig. 13 shows the water budget terms for the same problem without accounting for the oxic and anoxic points as limiting considerations to transpiration. A saturation value greater than unity for oxic and anoxic points is used to disable this feature of the model. For this case, evapotranspiration increases steadily as

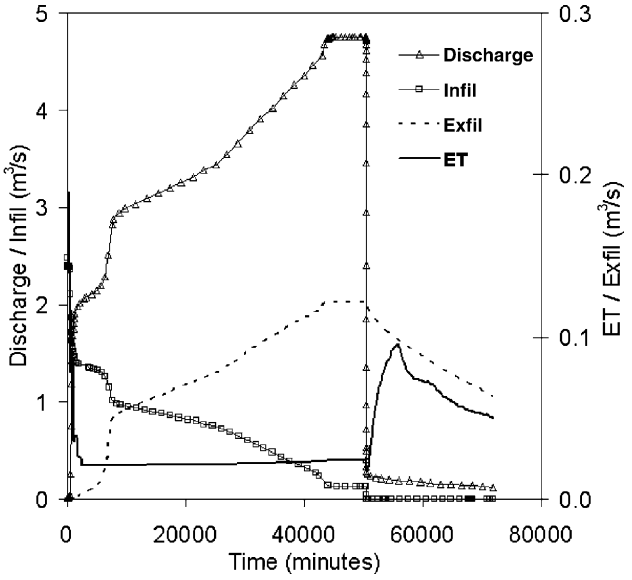

Fig. 12. Water budget components for simulation with evapotranspiration.

Table 1
Parameter values for evapotranspiration

Parameter	Value
Soil evaporation distribution function	
Overland flow plane	0.6
Soil layer 1	0.3
Soil layer 2	0.1
Soil layers 3–11	0.0
Root zone distribution function	
Soil layer 1	0.6
Soil layer 2	0.3
Soil layer 3	0.07
Soil layer 4	0.03
Soil layers 5–11	0.0
Leaf area index	2.08
Reference evapotranspiration	3.0×10^{-7} m/s
Transpiration constants C_1, C_2 and C_3	0.3, 0.2, 3.0×10^{-6} m/s
Saturation at field capacity	0.32
Saturation at wilting point	0.2
Saturation at oxic limit	0.76
Saturation at anoxic limit	0.9
Energy limiting stage saturation	0.32
Evaporation limiting stage saturation	0.2

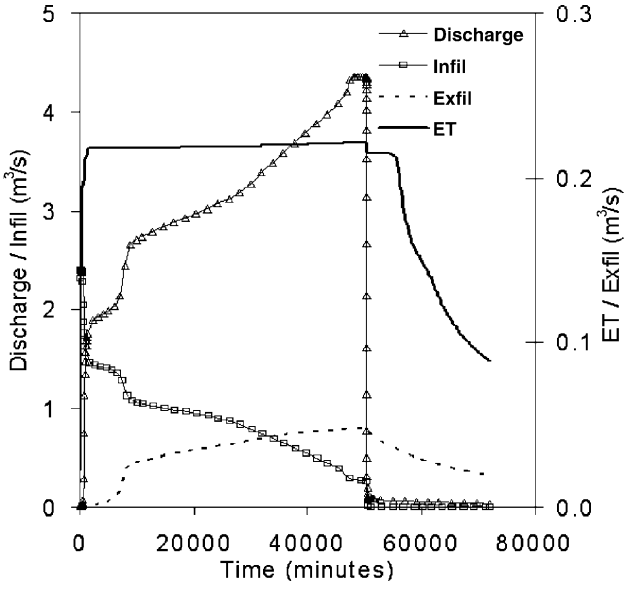

Fig. 13. Sensitivity of water budget components to anoxic moisture.

moisture in the upper layer increases, decreasing only when the recession period reduces moisture levels in the upper layers. For this case, the net evapotranspiration is about 10% of the total water budget, an effect that is reflected in the discharge and infiltration curves. Infiltration rates are higher at any time during the rainfall event to replenish water lost to evapotranspiration. As a result, the discharge rates are less at any given time than for the base case. Finally, it should be noted that the simulation with consideration of oxic and anoxic effects on the roots takes about 1.5 times longer than the base case simulation, whereas the simulation without these effects takes about 1.1 times longer.

4.4. Flood mitigation by flow-way alterations along a river

This problem examines the effects of engineered alterations made along a 40 km stretch of river on an incoming flood event. Fig. 14 schematically shows the pristine system and the existing engineered structures. Reach 1 in a hilly gorge flows into reach 2 on flatter terrain passing by a town with the potential for flooding. Reach 3 is an engineered flood bypass system with closed gates at its upstream end that are opened only when water levels at the town center reach a maximum allowable safe level (elevation of 361 m). Reach 3 merges with reach 2 into reach 4 along steeper terrain, which flows into reach 5 further downstream along flat terrain. At the downstream end of reach 4, an artificial reservoir is constructed for recreational and other purposes, by erection of an earth dam with a free-flowing weir system into reach 5. The system under analysis is discretized into 84 segments with 17, 20, 17, 12, and 18 segments in

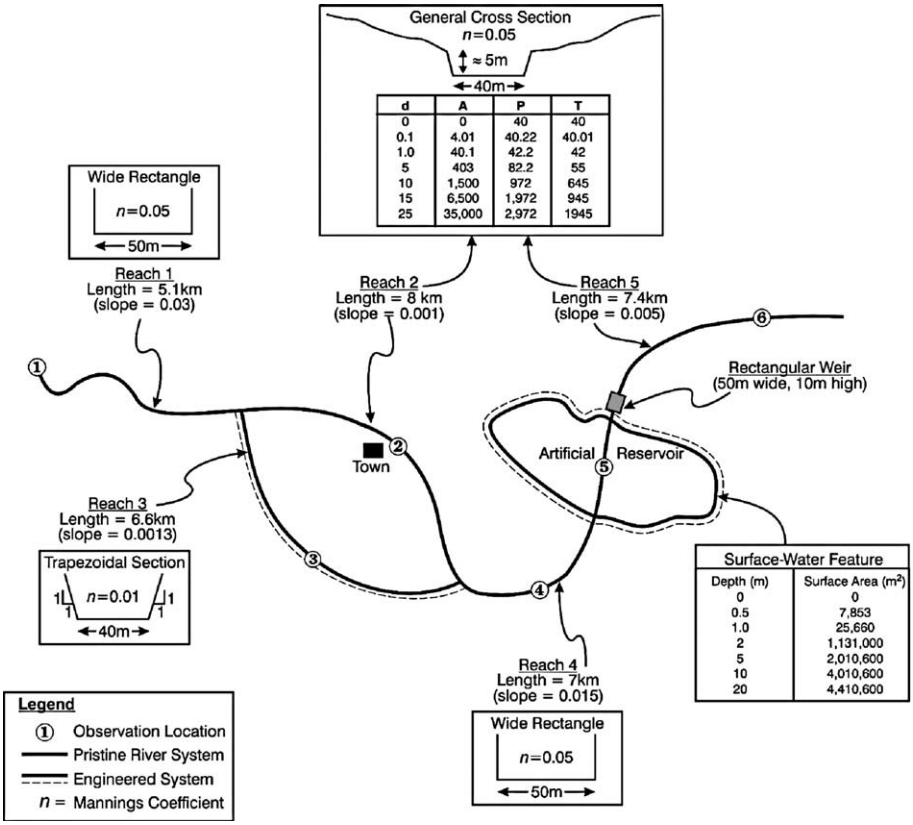

Fig. 14. Schematic representation of river and engineered system.

reaches 1, 2, 3, 4, and 5 respectively ranging in length from 130 to 630 m except for the artificial reservoir which submerges 2360 m of pristine river system. Fig. 15 shows the breakthrough of the simulated flood event at select observation points as located in Fig. 14. The flux at observation location 1 at the upstream end of the domain is the input driving force; water exits the downstream end of the domain under critical depth flow conditions. The rest of the stage and discharge breakthrough curves in Fig. 15 depict simulation results for pristine and engineered conditions. Flow and stage conditions before and during the flood are similar for pristine and engineered conditions at observation locations 1 and 6. For engineered conditions, the trigger level of 361 m is reached at 46 h in the town center (observation location 2) thus opening the bypass gates and averting the 364.7 m stage flood of pristine conditions. Flow at observation location 4 in reach 4 is not significantly affected by the engineered system, aside from the initial shock of opening the gates. The stage at observation location 5 (site of the artificial reservoir) is raised by about 3 and 2 m before and during the flood respectively, due to the weir. Both simulations take only seconds to run on a desktop computer; therefore, simulation times are judged by the number of time-steps taken to complete the 100 h simulation duration. The engineered system's simulation is 1.16 times longer, resulting from resolving the initial shock when the gate is instantly opened. Finally, note that the flood volume is significantly larger than reservoir capacity; therefore,

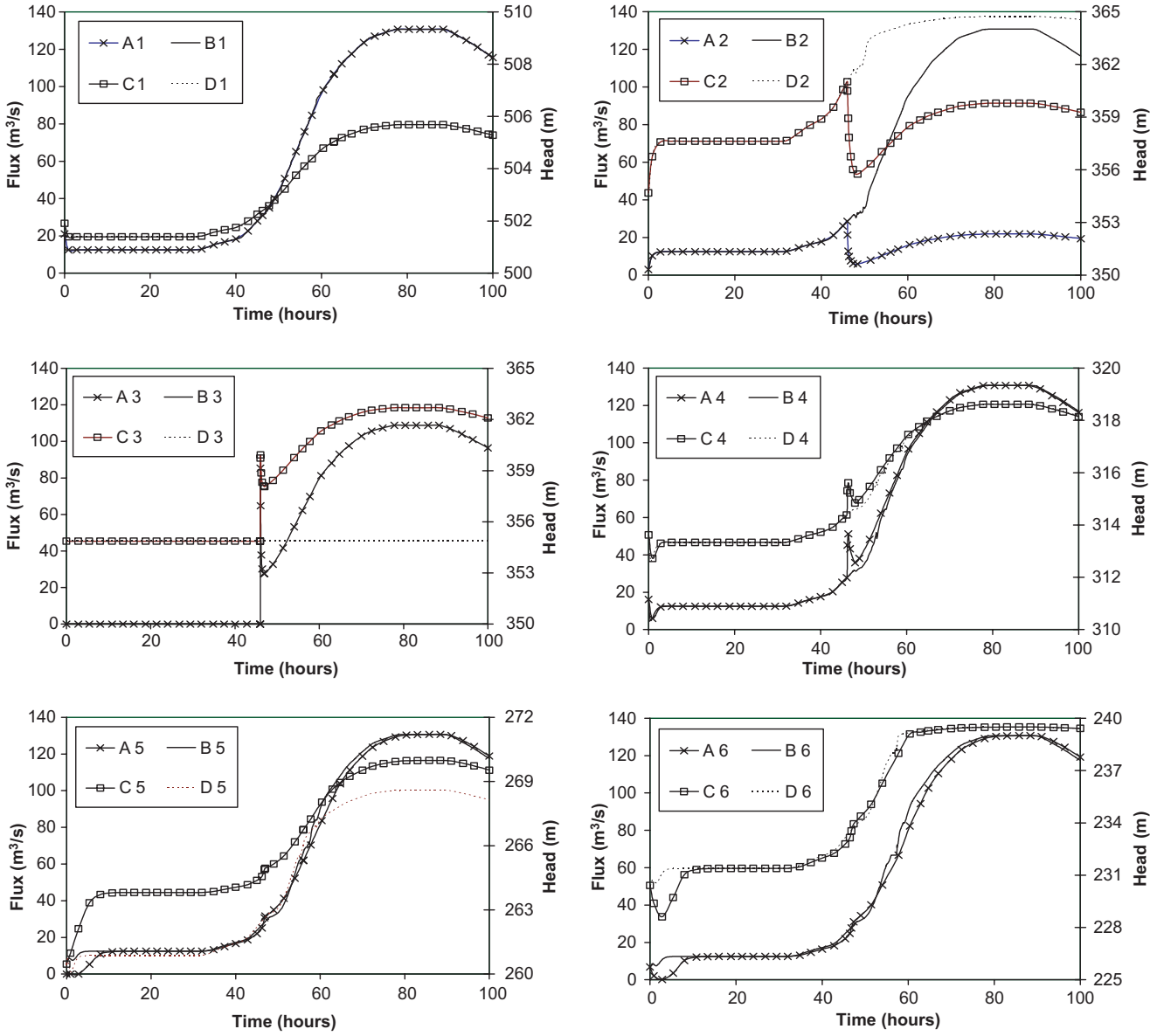

Fig. 15. Breakthrough curves of stage and discharge for flood event at the various observation locations. (A, engineered flux; B, pristine flux; C, engineered stage; D, pristine stage.)

the weir has little downstream mitigating effect at observation location 6.

5. Conclusions

A fully-coupled, physically-based, spatially-distributed model of conjunctive surface/subsurface flow has been presented. The model includes a fully three-dimensional solution for saturated–unsaturated flow in the subsurface coupled with two- and one-dimensional solutions for surface-water flow; the two-dimensional solutions represent overland runoff, and the one-dimensional solutions represent flow within and through surface-water features such as rivers, canals, pipes, lakes and ponds that are of a much smaller dimension than that of the simulation. Other scale-dependent features of the model include depression storage and obstruction storage exclusion which affect surface-water flow and storage and surface/subsurface interactions in a physically-based fashion. The model also incorporates control features for flow through rivers and streams to include the effects of bridges, culverts, manholes, weirs, and pump-stations in a simulation.

The governing equations are solved using current state-of-the-art techniques designed for highly non-linear complex situations. Treatment of the conductance terms in the overland flow equations is crucial in obtaining physically correct solutions in a robust and efficient manner. The domains are fully coupled, or may be linked in an iterative or time-lagged manner. Example problems demonstrate the effects of various physical parameters to the flow system, as well as the potential disadvantages of using linked solutions for complex problems with large interaction fluxes. The last example problem discussed also demonstrates the model's ability to simulate regulated engineered systems for flood control or agricultural purposes. The model is currently being applied for conjunctive water management evaluations, and similar behavior is noted (with respect to results as well as numerical behavior) as for the examples shown here. It is therefore important to understand system responses and simulation behavior for simplified elements of a model before attempting comprehensive analysis of large complex systems.

References

[1] Akan AO, Yen BC. Mathematical model of shallow water flow over porous media. J Hydraul Div 1981;107(HY4):479–94.

[2] Allen RG, Pereira LS, Raes D, Smith M. Crop evapotranspiration, Guidelines for computing crop water requirements, FAO Irrigation and Drainage paper 56, Food and Agriculture Organization of the United Nations, Rome, 1998.

[3] Bicknell BR, Imhoff JL, Kittle JL, Donigian AS, Johanson RC. Hydrological Simulation Program FORTRAN (HSPF): User's Manual for Release 10, EPA-600/R-93/174, US Environmental Protection Agency, Athens, GA, 1993.

[4] Brooks RH, Corey AT. Properties of porous media affecting fluid flow. ASCE J Irrig Drain Div 1966;92(IR2):61–88.

[5] Celia MA, Bouloutas ET, Zarba RL. A general mass-conservative numerical solution for the unsaturated flow equation. Water Resour Res 1990;27(7):1483–96.

[6] Chaudhry MH. Open-channel flow. Englewood Cliffs, NJ: Prentice-Hall; 1993.

[7] Crawford NH, Linsely RK. Digital simulation in hydrology: Stanford watershed model IV, Technical Report No. 39, Department of Civil Engineering, Stanford University, Stanford, CA, 1966.

[8] diGiammarco P, Todini E, Lamberti P. A conservative finite element approach to overland flow: the control volume finite element formulation. J Hydrol 1996;175:267–91.

[9] Fairbanks J, Panday S, Huyakorn PS. Comparisons of linked and fully coupled approaches to simulating conjunctive surface/subsurface flow and their interactions. In: Seo, Poeter, Zheng, Poeter, editors. MODFLOW 2001 and Other Modeling Odysseys—Conference Proceedings, Golden, CO; 2001. p. 356–61.

[10] Feddes RA, Kowalik PJ, Zaradny H. Simulation of field water use and crop yield. New York: John Wiley and Sons; 1978.

[11] Fennema RJ, Chaudhry MH. Explicit methods for two-dimensional unsteady free-surface flows. J Hydr Engrg ASCE 1990;116(8):1013–34.

[12] Fiedler FR, Ramirez JA. A numerical method for simulating discontinuous shallow flow over an infiltrating surface. Int J Numer Meth Fluids 2000;32:219–40.

[13] Forsyth PA, Wu YS, Pruess K. Robust numerical methods for saturated–unsaturated flow with dry initial conditions in heterogeneous media. Adv Water Resour 1995;18:25–38.

[14] Freeze RA. Role of subsurface flow in generating surface runoff. 1. Base flow contributions to channel flow. Water Resour Res 1972;8:609–23.

[15] Freeze RA. Role of subsurface flow in generating surface runoff. 2. Upstream source areas. Water Resour Res 1972;8:1272–83.

[16] Gottardi G, Venutelli M. A control-volume finite-element model for two-dimensional overland flow. Adv Water Resour 1993;16:277–84.

[17] Govindaraju RS, Kavvas ML. Dynamics of moving boundary overland flows over infiltrating surfaces at hillslopes. Water Resour Res 1991;27(8):1885–98.

[18] Graham DN, Refsgaard A. MIKE SHE: a distributed, physically based modeling system for surface water/groundwater interactions. In: Seo, Poeter, Zheng, Poeter, editors. MODFLOW 2001 and Other Modeling Odysseys—Conference Proceedings, Golden, CO; 2001. p. 321–7.

[19] HydroGeoLogic. MODHMS: a comprehensive MODFLOW-based hydrologic modeling system, Version 1.1, Code documentation and user's guide. HydroGeoLogic Inc., Herndon, VA, 2000.

[20] Huyakorn PS, Pinder GF. Computational methods in subsurface flow. London: Academic Press; 1983.

[21] Huyakorn PS, Springer EP, Guvanasen V, Wadsworth TD. A three dimensional finite element model for simulating water flow in variably saturated porous media. Water Resour Res 1986;22(12):1790–808.

[22] Kristensen KJ, Jensen SE. A model for estimating actual evapotranspiration from potential evapotranspiration. Nordic Hydrol 1975;6:170–88.

[23] LaBolle EM, Fogg GE. A review of California's integrated groundwater and surface-water model (ISGM). In: Seo, Poeter, Zheng, Poeter, editors. MODFLOW 2001 and Other Modeling Odysseys—Conference Proceedings, Golden, CO; 2001. p. 349–55.

[24] McDonald MG, Harbaugh AW. A modular three-dimensional finite-difference groundwater flow model. US geological survey techniques of water-resources investigations, Book 6; 1988. 586 p [chapter A1].
[25] Monteith JL. Evaporation and surface temperature. Q J R Meteorol Soc 1981;107:1–27.
[26] Morita M, Yen BC. Numerical methods for conjunctive two-dimensional surface and three-dimensional sub-surface flows. Int J Numer Meth Fluids 2000;32:921–57.
[27] Panday S, Huyakorn PS, Therrien R, Nichols RL. Improved three-dimensional finite-element techniques for field simulation of variably saturated flow and transport. J Contam Hydrol 1993;12:3–33.
[28] Pinder GF, Sauer SP. Numerical simulation of flow wave modification due to back storage effects. Water Resour Res 1971;7(1):63–70.
[29] Prudic DE. Documentation of a computer program to simulate stream-aquifer relations using a modular, finite-difference, ground-water flow model. US Geological Survey Open-File Report 88–729; 1989. 113 p.
[30] Roberson JA, Crowe CT. Engineering fluid mechanics. third ed. Boston: Houghton Mifflin Company; 1985.
[31] Schaffranek RW, Baltzer RA, Goldberg DE. A model for simulation of flow in singular and interconnected channels. Techniques of water-resources investigations of the US geological survey, Book 7; 1981. 110 p [chapter C3].
[32] Senarath SUS, Ogden FL, Downer CW, Sharif HO. On the calibration and verification of two-dimensional, distributed, Hortonian, continuous watershed models. Water Resour Res 2000;36(6):1495–510.
[33] Singh V, Bhallamudi SM. Hydrodynamic modeling of basin irrigation. J Irrig Drain Engrg ASCE 1997;123(6):407–14.
[34] Singh V, Bhallamudi SM. Conjunctive surface–subsurface modeling of overland flow. Adv Water Resour 1998;21:567–79.
[35] Smith RE, Goodrich DC, Quinton JN. Dynamic, distributed simulation of watershed erosion: The KINEROS2 and EUROSEM models. J Soil Water Conserv 1995;50(5):517–20.
[36] Swain ED, Wexler EJ. A coupled surface-water and ground-water flow model for simulation of stream–aquifer interaction. US geological survey techniques of water-resources investigations, Book 6; 1996. 125 p [chapter A6].
[37] USACE. HEC-1: Flood Hydrograph Package, User's Manual, Version 4.1, US Army Corps of Engineers, Hydrologic Engineering Center, Davis, CA, 1998.
[38] USACE. UNET: One-dimensional unsteady flow through a full network of open channels, User's Manual. US Army Corps of Engineers, Hydrologic Engineering Center, Davis, CA, 1997.
[39] VanderKwaak JE. Numerical simulation of flow and chemical transport in integrated surface–subsurface hydrologic systems, Doctorate Thesis, Department of Earth Sciences, University of Waterloo, Ontario, Canada, 1999.
[40] VanderKwaak JE, Loague K. Hydrologic-response simulations for the R-5 catchment with a comprehensive physics-based model. Water Resour Res 2001;37(4):999–1013.
[41] van Genuchten MTh, Pinder GF, Saukin WP. Modeling of leachate and soil interactions in an aquifer, Management of Gas and Leachate in Landfills. US Environmental Protection Agency, Rep. EPA-600/9-77-026; 1977. p. 95–103.
[42] van Genuchten MTh. A closed-form equation for predicting the hydraulic conductivity of unsaturated soils. Soil Sci Soc Am J 1980;44:892–8.
[43] Walton R, Wexler EJ, Chapman RS. An integrated groundwater/open channel flow model, Technical Report, West Consultants Inc., Bellevue, WA, and Gartner Lee, Toronto, Canada, 1999.
[44] Wigmosta MS, Vail LW, Lettenmaier DP. A distributed hydrology-vegetation model for complex terrain. Water Resour Res 1994;30(6):1665–79.
[45] Woolhiser DA, Smith RE, Giraldez J-V. Effects of spatial variability of saturated hydraulic conductivity on Hortonian overland flow. Water Resour Res 1997;32(3):671–8.
[46] Woolhiser DA, Smith RE, Goodrich DC. KINEROS, a kinematic runoff and erosion model, Documentation and user manual, USDA—Agricultural Research Service, ARS-77; 1990. 130 p.
[47] Zhang W, Cundy TW. Modeling of two-dimensional overland flow. Water Resour Res 1989;25(9):2019–35.